stretching vibration at 1560 cm^{-1} was measured with a Miran 1A variable filter infrared spectrometer from Wilks Scientific Corp. A typical procedure is as follows: dry *n*-heptane (17.12 mL, cooled to 0 °C) and a solution of borinane in *n*-heptane (7.34 mL of 0.341 M in dimer at 0 °C) were taken in an oven-dried, nitrogen-cooled, 50-mL flask equipped with a connecting tube. The resulting solution was allowed to equilibrate at 0.0 °C ± 0.05 in a constant-temperature bath. The reaction was started by adding cyclopentene (0.44 mL). The reaction mixture, 0.200 M in cyclopentene and 0.100 M in borinane dimer, was pumped through a 0.1-mm Wilks NaCl IR cell at a rate of 4 mL/min using a FMI pump. The IR cell was kept at the reaction temperature by circulating water at 0 °C through a cell holder. The absorbance was recorded as a function of time on a strip chart recorder. After the reaction was complete, the background absorbance of the pure solvent was noted. The calculations of the rate constants were made by the procedure given in ref 1b.

Relative Reactivities. The procedure to determine the relative reactivity of alkenes A and B is as follows: 5.0 mmol each of alkenes A and B and a suitable internal standard (*n*-octane, 0.4 mL) were added to *n*-heptane (15 mL) in an oven-dried, nitrogen-cooled reaction flask fitted with a connecting tube. Several minute aliquots (1 μL) were removed and analyzed by GC to determine the response factors of the two alkenes using an SE-30 column (6 ft × 0.25 in.) on Chromosorb W. The mixture was cooled to 0 °C, and borinane (5.0 mmol) in *n*-heptane was added. The reaction temperature was kept at 0 °C. After the reaction was over, samples were removed and analyzed by GC to determine the amounts of unreacted alkenes. From the initial and final quantities of alkenes, the relative reactivity was calculated by using the Ingold–Shaw expression[20] (eq 7)

$$\frac{k_A}{k_B} = \frac{\ln [A]_o - \ln [A]_f}{\ln [B]_o - \ln [B]_f} \quad (7)$$

where $[A]_o$ and $[A]_f$ are the initial and final quantities in mmol of the alkene A and $[B]_o$ and $[B]_f$ are the corresponding quantities (in mmol) of the alkene B. The alkene pairs studied were 2-methyl-1-pentene/cycloheptene, 1-hexene/cycloheptene, cyclooctene/cycloheptene, cycloheptene/*cis*-3-hexene, *cis*-3-hexene/cyclopentene, cyclopentene/2-methyl-2-butene, 2-methyl-2-butene/*trans*-3-hexene, *trans*-3-hexene/1-methylcyclopentene, 1-methylcyclopentene/2,3-dimethyl-2-butene, 2,3-dimethyl-2-butene/cyclohexene; cyclohexene/1-methylcyclohexene, 1-methylcyclooctene/cycloheptene, *cis*-2-butene/2-methyl-2-butene, 2-methyl-2-butene/*trans*-2-butene, cycloheptene/3,3-dimethyl-1-butene.

(17) Value reported for *cis*-2-pentene vs. 2-methyl-2-pentene; ref 13.
(18) Value for *cis*-3-hexene vs. 2-methyl-2-butene.

Acknowledgment. Financial assistance from the National Science Foundation (Grant CHE 79-18881) is gratefully acknowledged.

Registry No. 1, 40209-82-3; 9-BBN, 280-64-8; Sia_2BH, 1069-54-1; $ThxBHCl{\cdot}SMe_2$, 75067-06-0; $Br_2BH{\cdot}SMe_2$, 55671-55-1; 2-methyl-1-pentene, 763-29-1; cyclooctene, 931-88-4; 1-hexene, 592-41-6; cycloheptene, 628-92-2; 1-methylcyclooctene, 933-11-9; 3,3-dimethyl-1-butene, 558-37-2; *cis*-3-hexene, 7642-09-3; *cis*-2-butene, 590-18-1; cyclopentene, 142-29-0; 2-methyl-2-butene, 513-35-9; *trans*-2-butene, 624-64-6; *trans*-3-hexene, 13269-52-8; 1-methylcyclopentene, 693-89-0; 2,3-dimethyl-2-butene, 563-79-1; cyclohexene, 110-83-8; 1-methylcyclohexene, 591-49-1.

(19) The hydroboration product of 1-methylcyclooctene with diborane undergoes rapid isomerization around the cyclooctane ring (Brown, H. C.; Zweifel, G. *J. Am. Chem. Soc.* **1961**, *83*, 2544–2557). With borinane and 1-methylcyclooctene, no isomerization of the organoborane is observed, even after prolonged intervals of time (48 h) at the reaction temperature (0 °C). Again, isomerization does not occur during the hydroboration of this alkene with 9-BBN (Taniguchi, H.; Brener, L.; Brown, H. C. *Ibid.* **1976**, *98*, 7107).
(20) Ingold, C. K.; Shaw, F. R. *J. Chem. Soc.* **1927**, 2918.

Steric and Electronic Effects in Ligand Substitution of Metal Carbonyls. Rapid Kinetics of Labile Carbonylmanganese Complexes by Transient Electrochemical Techniques

P. M. Zizelman, C. Amatore, and J. K. Kochi*

Contribution from the Department of Chemistry, Indiana University, Bloomington, Indiana 47405. *Received October 17, 1983*

Abstract: The ligand substitution kinetics of a series of carbonylmanganese cations $MeCpMn(CO)_2L^+$ with L = 3- and 4-substituted pyridine ligands are measured for a variety of phosphine nucleophiles N of differing steric and electronic properties. The unified free energy relationship in eq 17 is shown for the first time to accommodate all the extensive rate data, if the steric effect is evaluated by Tolman's cone angles for the phosphines, and the electronic effects are evaluated by the acid–base dissociation constants of the pyridine ligands and the phosphine nucleophiles. The range of second-order rate constants k_1 for ligand substitution of $MeCpMn(CO)_2L^+$ extends over four decades from 3.0 to 2×10^4 M^{-1} s^{-1}. The strong dependence of log k_1 on both the electronic and steric effects of the pyridine ligand L and the phosphine nucleophile N points to an associative S_N2 mechanism for this ligand substitution. The measurement of the fast rates of ligand substitution by transient electrochemical techniques is based on the novel electrocatalysis of the neutral precursor $MeCpMn(CO)_2L$ in the presence of added phosphine nucleophiles, as described in Scheme I. The analysis of the electrochemical kinetics for this mechanism by Feldberg's method for the computer simulation of the cyclic voltammograms and by Saveant's adimensional evaluation of the CV peak currents is described in detail.

The mechanism of ligand substitution of metal carbonyls is central to the successful catalysis of a variety of important processes leading to the reduction of carbon monoxide.[1,2] As such, ligand exchange in metal carbonyls and their derivatives has received extensive mechanistic scrutiny.[3-5] The generally accepted mechanisms for the displacement of the ligand L from a series of metal carbonyls $L{-}M(CO)_n$ by added nucleophiles N such as amines, phosphines, etc., involve diamagnetic intermediates,

* Present address: Department of Chemistry, University of Houston, University Park, Houston, Texas 77004.

(1) Wender, I.; Pino, P.; Eds. "Organic Synthesis via Metal Carbonyls"; Wiley-Interscience: New York, (a) 1968; Vol. 1; (b) 1976; Vol. 2.
(2) (a) Pruett, R. L. *Adv. Organomet. Chem.* **1979**, *17*, 1. Forster, D. *Ibid.* **1979**, *17*, 255. Masters, C. *Ibid.* **1979**, *17*, 61. (b) Heck, R. F. "Organotransition Metal Chemistry"; Academic Press: New York, 1974.
(3) Basolo, F.; Pearson, R. G. "Mechanisms of Inorganic Reactions"; 2nd ed.; Wiley-Interscience: New York, 1967; p 533.

0002-7863/84/1506-3771$01.50/0

generally with 16- and 18-electron configurations, in competing dissociative and associative processes.[5,6] However, there are recent

$$L\text{-}M(CO)_n + N \rightarrow N\text{-}M(CO)_n + L$$

reports of ligand substitution in metal carbonyls proceeding via odd-electron, paramagnetic intermediates.[7,8] In particular, it has been demonstrated that the facile substitution of nitrogen-centered ligands such as acetonitrile and pyridine in such molybdenum, tungsten, and manganese carbonyls as $L\text{-}M(CO)_n$ = *fac*-$(MeCN)_3W(CO)_3$, *cis*-$(py)_2Mo(CO)_4$, and $(\eta^5\text{-}C_5H_4Me)Mn(CO)_2(py)$ by added phosphines and isonitriles is actually a chain process which proceeds via the 17-electron radical cations, *fac*-$(MeCN)_3W(CO)_3^+$, $(\eta^5\text{-}C_5H_4Me)Mn(CO)_2(py)^+$, etc.[9,10]

In a previous study we described an extremely efficient chain mechanism for the substitution of various metal carbonyl derivatives $L\text{-}M(CO)_n$ by different nucleophiles (N) which proceeds via the labile 17-electron cation radical $L\text{-}M(CO)_n^+$.[11] The catalytic process could be initiated both chemically and electrochemically. Following either method of initiation, the propagation steps have been shown to involve two fundamental reactions, viz. ligand substitution:

$$L\text{-}M(CO)_n^+ + N \rightarrow N\text{-}M(CO)_n^+ + L \qquad (1)$$

electron transfer:[12]

$$N\text{-}M(CO)_n^+ + L\text{-}M(CO)_n \rightarrow N\text{-}M(CO)_n + L\text{-}M(CO)_n^+ \qquad (2)$$

The net process represents ligand substitution of the metal carbonyl itself, i.e.

overall:

$$L\text{-}M(CO)_n + N \rightarrow N\text{-}M(CO)_n + L \qquad (3)$$

and it has a high catalytic turnover number, e.g., the current efficiency for the electrocatalysis exceeding 10^3.

The ligand substitution of the cation radical $L\text{-}M(CO)_n^+$ in eq 1 is of particular interest since the second-order rate constant can easily exceed 10^4 M^{-1} s^{-1}, which is more than 6 decades faster than that of its diamagnetic precursor $L\text{-}M(CO)_n$ in eq 3. This facile process offers us an excellent opportunity to examine the structural effects of the leaving ligand (L) and the entering nucleophile (N) on the rate of ligand substitution, by systematically varying both their steric and electronic properties. However, rapid reactions with rate constants of this magnitude are difficult to measure by conventional methods. Accordingly, our second objective in this report is to show how transient electrochemical techniques such as cyclic voltammetry (CV), which utilize readily available instrumentation, can be employed to measure such rate constants routinely.

Results

We begin by noting that a solution of the carbonylmanganese derivative $MeCpMn(CO)_2py$ is stable in the presence of added phosphine nucleophiles (PR_3). However, the admission of traces of air or the passage of a trickle of electrical current through the solution is sufficient to convert it completely to the substitution product $MeCpMn(CO)_2PR_3$ within 10 min at room temperature. The electrocatalytic phenomenon is clearly revealed in the series of (initial anodic scan) cyclic voltammograms shown in Figure 1. The first row (a) of cyclic voltammograms taken at several scan rates relates to the reversible redox process:

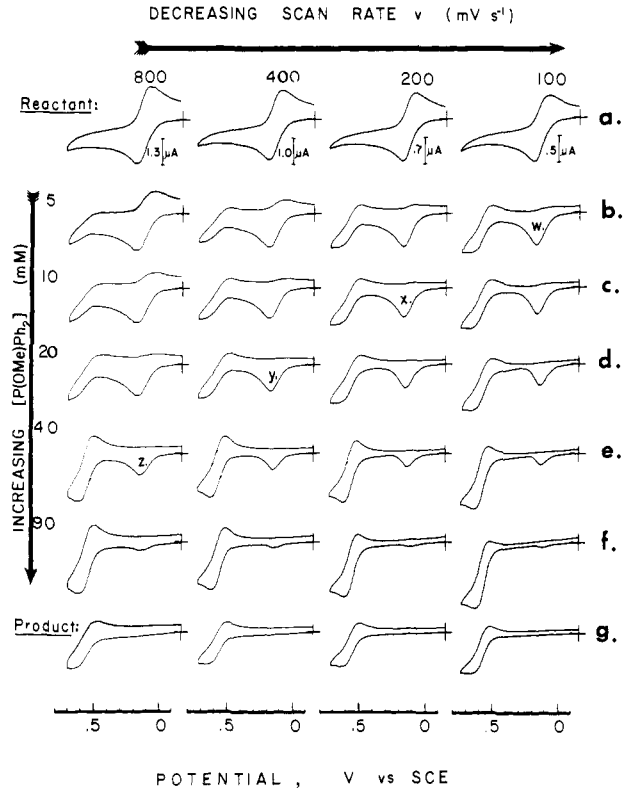

Figure 1. (Row a) The cyclic voltammograms obtained on the initial anodic scan of 1.2×10^{-3} M $MeCpMn(CO)_2$(4-Acpy) in CH_2Cl_2 containing 0.1 M TBAP at various scan rates. (Rows b–f) The cyclic voltammograms of the same solution in (a) but containing successively increasing amounts of the phosphine $P(OMe)Ph_2$, as indicated. (Row g) The cyclic voltammograms of 8.4×10^{-4} M $MeCpMn(CO)_2[P(OMe)Ph_2]$ in CH_2Cl_2 containing 0.1 M TBAP at various scan rates.

$$MeCpMn(CO)_2py \overset{E_R^0}{\rightleftharpoons} MeCpMn(CO)_2py^+ + e \qquad (4)$$

Similarly, the last row (g) of reversible cyclic voltammograms represents the redox process of the substitution product $MeCpMn(CO)_2PR_3$, i.e.

$$MeCpMn(CO)_2PR_3 \overset{E_P^0}{\rightleftharpoons} MeCpMn(CO)_2PR_3^+ + e \qquad (5)$$

which was unambiguously synthesized by an independent procedure. The series of cyclic voltammograms in rows b to f were obtained from solutions of $MeCpMn(CO)_2py$ containing successively higher concentrations of added phosphine.

Examination of this matrix of cyclic voltammograms, a seriatim, provides unique insight into the mechanism of the electrocatalytic ligand substitution. [Note the anodic (R) and cathodic (R^+) currents are directly related to the concentrations of the reactant $MeCpMn(CO)_2py$ and its cation radical $MeCpMn(CO)_2py^+$, respectively, in the region about the electrode.] Thus the vertical columns of cyclic voltammograms in Figure 1 show that [$MeCpMn(CO)_2py$] decreases dramatically in the presence of incremental additions of phosphine, and it is replaced by an equivalent amount of the product $MeCpMn(CO)_2PR_3$. Moreover, the CVs in rows b through f indicate that the same variation in the relative concentrations of the reactant and product can be achieved simply by changing the CV sweep rate v. [For example, compare the CVs labelled w, x, y, and z along the diagonal.] The lifetime of the initially formed cation radical $MeCpMn(CO)_2py^+$ is exceedingly short in the presence of added phosphine, as seen

(4) (a) Dobson, G. R. *Acc. Chem. Res.* **1976**, *9*, 300. (b) Deeming, A. J. *Inorg. React. Mech.* **1981**, *7*, 275 and related reviews in this series.
(5) (a) Darensbourg, D. J. *Adv. Organomet. Chem.* **1982**, *21*, 113. (b) Atwood, J. D.; Wovkulich, M. J.; Sonnenberger, D. C. *Acc. Chem. Res.* **1983**, *16*, 350.
(6) Cotton, F. A.; Wilkinson, G. "Advanced Inorganic Chemistry"; 4th ed.; Wiley: New York, 1981; p 1185 ff.
(7) McCullen, S. B.; Walker, H. W.; Brown, T. L. *J. Am. Chem. Soc.* **1982**, *104*, 4007.
(8) Shi, Q.; Richmond, T. G.; Trogler, W. C.; Basolo, F. *J. Am. Chem. Soc.* **1982**, *104*, 4032.
(9) Hershberger, J. W.; Klingler, R. J.; Kochi, J. K. *J. Am. Chem. Soc.* **1982**, *104*, 3034.
(10) Hershberger, J. W.; Kochi, J. K. *J. Chem. Soc., Chem. Commun.* **1982**, 212.
(11) Hershberger, J. W.; Klingler, R. J.; Kochi, J. K. *J. Am. Chem. Soc.* **1983**, *105*, 61.
(12) For the contribution by electron transfer to and from the electrode see Figure 12, in the Experimental Section.

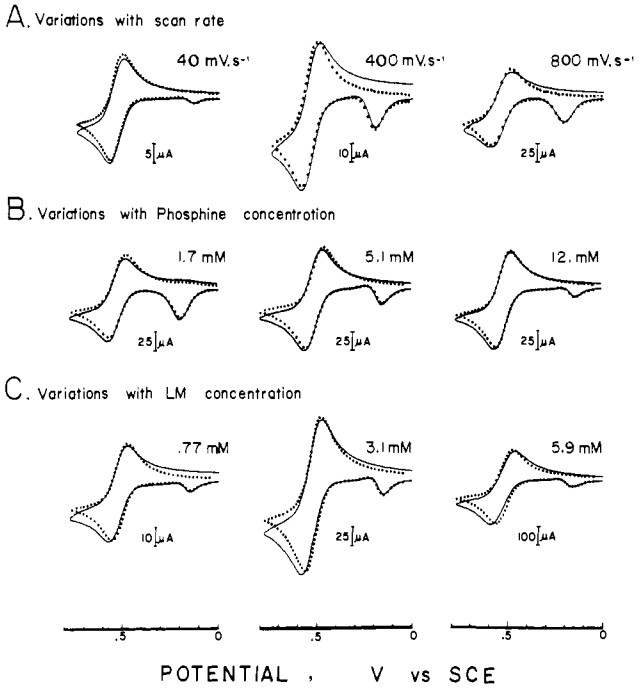

Figure 2. Comparisons of the experimental (solid curve) and theoretical (filled circles) cyclic voltammograms of $MeCp(CO)_2(NCMe)$ with PPh_3 as a function of the scan rate v in row A, phosphine concentration, [N], in row B, and metal carbonyl concentration [L–M] in row C by the use of a single set of kinetic parameters: $k_1 = 1.3 \times 10^4$ M^{-1} s^{-1} and $k_2 = 5 \times 10^5$ M^{-1} s^{-1}.[13]

by the return cathodic wave R^+, which is either severely diminished or absent (see particularly the CV in column 4 of row f). One is thus forced to the conclusion that electrocatalysis stems from the lability of the reactant cation $MeCpMn(CO)_2py^+$ to ligand substitution, as in eq 1. Furthermore, the direction of the current flow (i.e., anodic) demonstrates that the product is produced in the reduced form by an electron-transfer process, as in eq 2.

Having described the electrocatalytic phenomenon by bulk and transient electrochemical methods, we turn to the quantitative description of the kinetics associated with ligand substitution of metal carbonyls. In particular, let us now consider how the computer simulation of the experimental cyclic voltammograms can be used to extract the desired second-order rate constant for ligand substitution in eq 1 from the complex kinetics of electrocatalysis. We proceed from the established mechanism in Scheme I, which includes the ligand substitution and electron-transfer steps in eq 1 and 2, respectively, together with the electrode processes for the carbonylmetal reactant (eq 4) and its substitution product (eq 5).[11,13] [For convenience in the presentation, the reactant and the substitution product have been abbreviated as L–M and N–M, respectively, and the appropriate rate constant labeled for each step.] The details of the construction of the theoretical cyclic

Scheme I

$$L\text{–}M \overset{E_R^0}{\rightleftharpoons} L\text{–}M^+ + e \tag{6}$$

$$L\text{–}M^+ + N \underset{k_{-1}}{\overset{k_1}{\rightleftharpoons}} N\text{–}M^+ + L \tag{7}$$

$$N\text{–}M^+ + L\text{–}M \xrightarrow{k_2} N\text{–}M + L\text{–}M^+, \text{ etc.} \tag{8}$$

$$N\text{–}M^+ + e \overset{E_P^0}{\rightleftharpoons} N\text{–}M \tag{9}$$

voltammograms by digital simulation of the kinetics according

(13) The other parameters used in the simulation were the following: $D = 2.4 \times 10^{-5}$ cm s^{-1}, $\beta = 0.5$, $k_s(MeCpMn(CO)_2(NCMe)) = 0.048$ cm s^{-1}, $k_s(MeCpMn(CO)_2PPh_3) = 0.023$ cm s^{-1}, as described in ref 11. The agreement between the experimental and simulated CVs implies that $k_{-1} = 0$, i.e., the ligand substitution is irreversible.

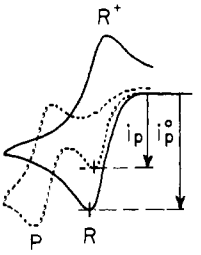

Figure 3. The current ratio i_p/i_p^0 of the anodic wave R in typical cyclic voltammograms of $MeCpMn(CO)_2py$ obtained in the presence (dashed curve) and absence (solid curve) of added phosphine.

to the mechanism in Scheme I are described in the Experimental Section.[14–16] A typical result is illustrated in Figure 2 for the cyclic voltammograms which pertain to the electrocatalytic substitution of different concentrations of $MeCpMn(CO)_2NCMe$ in the presence of varying amounts of added triphenylphosphine and at various sweep rates.[20] This series of cyclic voltammograms emphasizes that the anodic current ratio P/R is strongly dependent on the variations in the phosphine concentration and on the sweep rate (shown in rows A and B), but this ratio is quite independent of the initial concentration of L–M (see row C). It is singularly noteworthy that all the fits of the computer simulations with the experimental cyclic voltammograms, including those at different values of v, [N], and [L-M] in Figure 2, were derived from a *single set of kinetic parameters* in Scheme I, i.e., $k_1 = 1.3 \times 10^4$ M^{-1} s^{-1} and $k_2 = 5 \times 10^5$ M^{-1} s^{-1}. Thus the validity of Scheme I to quantitatively describe the kinetics of the electrocatalytic substitution in eq 3 is unmistakable. Important to our interest in this study is the finding that the optimization of the computer-simulated cyclic voltammograms is not critically dependent on the value of k_2 provided it is chosen over a range $10^4 < k_2 < 10^{10}$ M^{-1} s^{-1} for scan rates between 40 and 800 mV s^{-1}. As a result, the ligand substitution step in eq 7 is rate limiting, and the value of k_1 can be evaluated with a precision greater than 15% by the computer simulation technique. It follows that the rate law associated with the ligand substitution step in eq 7 is[22]

$$\partial[L\text{–}M^+]/\partial t = -k_1[L\text{–}M^+][N] \tag{10}$$

where the rate constant k_1 is independent of the concentration of the carbonylmetal precursor L–M as well as the CV scan rate. In other words, the concentration of $L\text{–}M^+$ in the region about the electrode is determined solely by the values of k_1, [N], and v.[20] [We will return to this important conclusion later.]

As effective as the CV simulation technique is for the determination of the desired rate constant k_1, it requires large amounts of computer time for the true iterative optimization of each system.[23] Therefore we considered an alternative approach which

(14) The computer simulation is based on Feldberg's method of finite differences.[15]

(15) (a) Feldberg, S. W., In "Electroanalytical Chemistry"; Bard, A. J., Ed.; Marcel Dekker: New York, 1969; Vol. 3, p 199. (b) Feldberg, S. W. In "Computer Application in Analytical Chemistry"; Mark, H. B., Ed.; Marcel Dekker: New York, 1972; Vol. 2, Chapter 7.

(16) The construction of theoretical cyclic voltammograms[14] in terms of a current–potential response arising from a particular mechanistic scheme such as that in Scheme I derives from the approach developed by Nicholson and Shain,[17] Matsuda,[18] and Savéant.[19]

(17) Nicholson, R. S.; Shain, I. *Anal. Chem.* **1964**, *36*, 706.

(18) Matsuda, H.; Ayabe, V. *Z. Elektrochem.* **1955**, *59*, 494.

(19) Savéant, J.-M. *Electrochim. Acta* **1967**, *12*, 999.

(20) In cyclic voltammetry, the time scale is given by the rate of mass transport to and from the electrode.[21] Thus, the cyclic voltammogram will depend on the rate of the chemical evolution of the intermediate relative to the rate of diffusion. Since the rate of diffusional mass transport is directly related to the scan rate v of the potential sweep, the variation of v affords unique information for which there is no counterpart in conventional kinetics.

(21) Amatore, C.; Savéant, J.-M. *J. Electroanal. Chem.* **1983**, *144*, 59 and references therein.

(22) The variation of $[L\text{–}M^+]$ with time as expressed in eq 10 refers only to those related to chemical processes in eq 7, and does not include changes arising from mass transport which are time and space dependent. See the Experimental Section for the complete expression for $\partial[L\text{–}M^+]/\partial t$.

(23) Furthermore, the "goodness of fit" of a theoretical CV to an experiment is difficult to define quantitatively, since the capacitive current and the background current of the medium are difficult to measure.

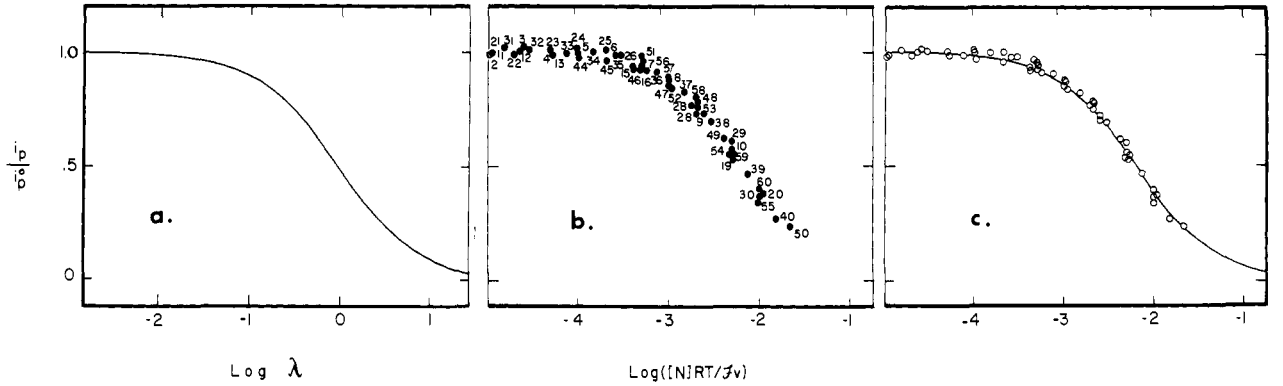

Figure 4. Variations of the peak current ratio i_p/i_p^0 with the adimensional parameter log λ = log $(k_1RT[N]/\mathcal{F}v)$ for the CVs obtained from the electrocatalytic ligand substitution of the pyridine derivatives of manganese carbonyls with phosphines. (a) Theoretical working curve based on the mechanism in Scheme I. (b) Experimental points obtained from the data in Table I showing variations in v, [L–M], and [N]. (c) Translation of the curve in (a) along the abscissa by 2.34 units (=log k_1) to coincide with the points in (b).

Table I. The Variation of the Anodic Peak Current Ratio i_p/i_p^0 for the Electrocatalytic Ligand Substitution of η^5-MeCpMn(CO)$_2$(py-Ac-4) by P(OMe)Ph$_2$ with the Experimental Variables of [LM], [N], and v

no.	[L–M] (10^3 M)	[N] (10^3 M)	v (V s^{-1})	$i_p/i_p^{0\,b}$	no.	[L–M] (10^3 M)	[N] (10^3 M)	v (V s^{-1})	$i_p/i_p^{0\,b}$
1	0.80	19.8_5	100	1.01	31	0.80	59.1	100	1.01
2	0.80	19.8_5	50	0.98	32	0.80	59.1	50	1.00
3	0.80	19.8_5	20	1.01_5	33	0.80	59.1	20	0.98_5
4	0.80	19.8_5	10	0.99	34	0.80	59.1	10	1.00
5	0.80	19.8_5	5	1.00	35	0.80	59.1	5	0.98
6	0.80	19.8_5	2	0.98	36	0.80	59.1	2	0.91
7	0.80	19.8_5	1	0.94_5	37	0.80	59.1	1	0.82_5
8	0.80	19.8_5	0.5	0.88_5	38	0.80	59.1	0.5	0.69
9	0.80	19.8_5	0.2	0.72_5	39	0.80	59.1	0.2	0.47
10	0.80	19.8_5	0.1	0.57	40	0.80	59.1	0.1	0.27
11	0.80	29.9	100	0.98_5	41	0.80	59.8	200	1.04
12	0.80	29.9	50	1.00	42	0.80	59.8	100	1.02
13	0.80	29.9	20	0.98_5	43	0.80	59.8	50	1.04
14	0.80	29.9	10	0.89	44	0.80	59.8	20	0.96_5
15	0.80	29.9	5	0.93	45	0.80	59.8	10	0.95_5
16	0.80	29.9	2	0.91	46	0.80	59.8	5	0.92
17	0.80	29.9	1	0.81	47	0.80	59.8	2	0.83_5
18	0.80	29.9	0.5	0.74_5	48	0.80	59.8	1	0.78
19	0.80	29.9	0.2	0.52_5	49	0.80	59.8	0.5	0.62
20	0.80	29.9	0.1	0.37_5	50	0.80	59.8	0.1	0.24
21	0.80	39.5	100	0.99	51	3.4	39.5	2	0.97_5
22	0.80	39.5	50	0.98	52	3.4	39.5	1	0.84_5
23	0.80	39.5	20	1.00	53	3.4	39.5	0.5	0.73
24	0.80	39.5	10	1.00	54	3.4	39.5	0.2	0.53_5
25	0.80	39.5	5	1.02	55	3.4	39.5	0.1	0.34
26	0.80	39.5	2	0.98	56	1.7	39.5	2	0.95
27	0.80	39.5	1	0.91_5	57	1.7	39.5	1	0.88
28	0.80	39.5	0.5	0.76_5	58	1.7	39.5	0.5	0.78
29	0.80	39.5	0.2	0.60_5	59	1.7	39.5	0.2	0.56
30	0.80	39.5	0.1	0.37	60	1.7	39.5	0.1	0.40

[a] In CH_2Cl_2 solution containing 0.1 M TBAP at 22 °C. [b] See the Experimental Section for the determination of the peak current ratio.

stems from the conclusion expressed in eq 10, viz., there is only one rate-limiting step in the electrocatalytic ligand substitution process. In particular, the results illustrated in Figures 1 and 2 emphasize that the absolute magnitude of the anodic peak current R of the CV wave of the reactant L–M is very sensitive to changes in the concentrations of L–M and N, as well as the CV scan rate. In fact, Saveant's method[24] for the adimensional analysis of the electrochemical kinetics in Scheme I shows that the effect of the experimental variables of concentration, [L–M] and [N], and sweep rate, v, on the cyclic voltammogram can be expressed in terms of a single variable $\lambda = k_1(RT/\mathcal{F}v)[N]$, where R, T, and $\mathcal{F}$ have their usual significance.[25] In order to utilize this procedure, we consider the change in the anodic peak current R of the reactant L–M, with and without added phosphine nucleophile N, as the ratio i_p/i_p^0 identified in Figure 3. The current ratio i_p/i_p^0 was computed numerically (see the Experimental Section) as a function of log λ in order to construct the theoretical working curve shown in Figure 4a. Similarly, the experimental current ratio i_p/i_p^0 was plotted vs. the closely related function log $(RT/\mathcal{F}v)[N]$ from the extensive CV data in Table I obtained at various scan rates, reactant [L–M], and nucleophile [N] for a typical system. The result is shown in Figure 4b. The discrepancy between the scales in Figure 4, parts a and b, along the abscissa represents log k_1. Therefore Figure 4a should be translatable along this axis until it coincides with Figure 4b. The result is shown in Figure 4c. The striking fit of all the experimental points to the theoretical working curve in Figure 4c is achieved with a single value of the rate constant log k_1 = 2.34.[27] Indeed, the concurrence

(24) See, e.g.: Savēant, J.-M.; Vianello, E. *Electrochim. Acta*, **1963**, *8*, 905 and ref 21.

(25) When there is only one rate-limiting step in a mechanism, the adimensional analysis of the equations for electrochemical diffusion shows that the experimental variables can be expressed by a single adimensional parameter taking into account all the experimental parameters which influence the behavior of the chosen experimental variable.[21,26]

(26) Amatore, C.; Savēant, J.-M. *J. Electroanal. Chem.* **1979**, *102*, 21.

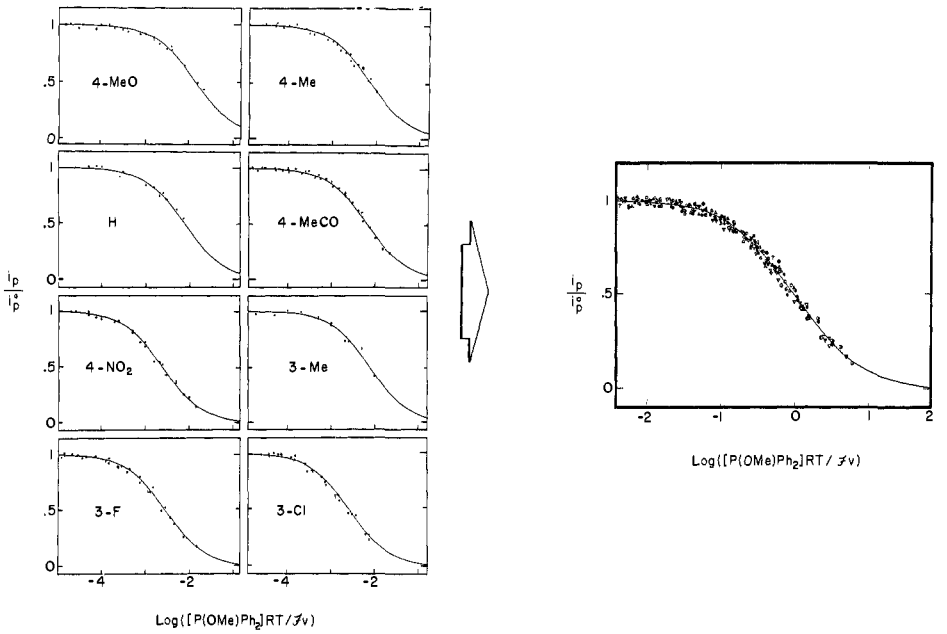

Figure 5. Unified pattern for the variation in the peak current ratio i_p/i_p^0 with the adimensional parameter log λ for the ligand substitution of various derivatives of $MeCpMn(CO)_2py$ by $P(OMe)Ph_2$. Left figures: Experimental data for 3- and 4-substituted pyridine ligands, as indicated. Right figure: Composite (filled circles) of all the data in the left figures, with each displaced by an amount corresponding to log k_1 along the abscissa to coincide with the theoretical working curve (solid line) in Figure 4a.

of the experimental parameters to afford a unique value of the rate constant provides another compelling confirmation of the validity of the electrochemical kinetics associated with the mechanism in Scheme I to describe the catalytic ligand substitution.[29] Moreover, it is important to note that the kinetics from Scheme I predict the reactant concentration [L–M] to be unimportant in the determination of k_1, as experimentally verified in Figure 2 (vide supra).

This convenient and rapid method of kinetic analysis was used to analyze the experimental i_p/i_p^0 data from the cyclic voltammograms of various meta- and para-substituted pyridine analogues of $MeCpMn(CO)_2py$ at different values of v, [L–M], and [N]. The results are shown on the left side of Figure 5. We wish to reemphasize that the remarkable fit of *all these data points* to the shape of the theoretical working curve (shown by the solid curve on the right side of Figure 5) confirms the general applicability of the adimensional method. It also establishes the validity of the mechanism in Scheme I to describe the electrocatalysis in terms of the rate-limiting ligand substitution of the carbonylmetal cation radical $L–M^+$. The second-order rate constants k_1 obtained in this manner are listed in Table II for the exchange of various substituted-pyridine ligands with the phosphine $P(OMe)Ph_2$ in the 17-electron cation radicals $MeCpMn(CO)_2(py\text{-}X)^+$, together with the acid–base dissociation constants of the free pyridines (indicated as pK_a^L).

Using the same method, we also examined the structural effect of the phosphine nucleophile on the rate constant k_1 for the 4-methoxy- and 4-nitropyridine derivatives of $MeCpMn(CO)_2py$, since they represent the opposite ends of the reactivity scale. The results are tabulated in Table III for various phosphines with differing electronic and steric effects, as indicated by the values of their acid–base dissociation constant pK_a^N and Tolman's cone angle θ, respectively.[30] Each rate constant listed in the table results from kinetic data obtained from testing an extensive series of the experimental variables of concentration and CV scan rates. Thus, the statistical treatment of more than 15 data points ensures that the variance in each rate constant (log k_1) is less than ±0.05.

Table II. Rate Constants for the Exchange of Substituted Pyridines by $P(OMe)Ph_2$ in the 17-Electron Cation Radicals η^5-$MeCpMn(CO)_2L^+$ [a]

no.	L	log k_1 [b]	k_1 (M^{-1} s^{-1}) [b]	pK_a^L [c]
1	4-methoxypyridine	1.88 (0.03)	75 (5)	6.58
2	4-methylpyridine	1.92 (0.06)	85 (10)	6.31 [d]
3	pyridine	2.11 (0.05)	130 (15)	5.21
4	4-acetylpyridine	2.34 (0.06)	220 (30)	3.51
5	4-nitropyridine	2.61 (0.06)	410 (45)	1.40
6	3-methylpyridine	2.10 (0.05)	125 (15)	5.67
7	3-fluoropyridine	2.55 (0.03)	345 (35)	3.36 [d]
8	3-chloropyridine	2.61 (0.04)	410 (40)	2.81

[a] In methylene chloride solutions containing ca. 10^{-3} M manganese carbonyl derivative, ca. 10^{-2} M $P(OMe)Ph_2$, and 0.1 M TBAP at 22 °C. [b] The number in parentheses represents the variance. [c] pK_a of the pyridinium/pyridine couple in water from ref 34. [d] Estimated value from ref 35 and 37.

Discussion

Electrochemical methods have provided an accurate and convenient measurement of an extensive series of rate constants k_1 for the rapid ligand substitution of different carbonylmanganese cations by various nucleophiles, i.e.,

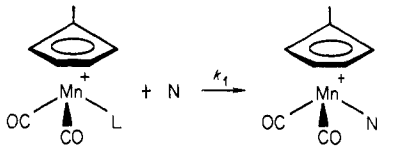

(11)

A survey of Tables II and III quickly reveals rate constants which vary drastically with the nature of the pyridine leaving group L and the entering phosphine nucleophile N. For example, a variation of k_1 by a factor of 10^4 is observed in proceeding from the displacement of L = 4-methoxypyridine by N = triphenylphosphine to the displacement of 4-nitropyridine by triethylphosphine. Since this rather extensive series represents various leaving groups and nucleophiles with regularly changing steric and electronic properties, it offers us an excellent opportunity to examine the mechanism of ligand substitution at a metal center. In particular, we wish to examine the quantitative relationship

(27) The best fit of the experimental data to the working curve is made by a statistical analysis designed to obtain the smallest value of the variance relative to the determination of log k_1 values. See ref 28.

(28) Bevington, P. R. In "Data Reduction and Error Analysis for the Physical Sciences"; McGraw-Hill: New York, 1969.

(29) In particular, it confirms rate constants k_2 for electron transfer to be $>10^8$ M^{-1} s^{-1} and that for eq 9 to be unimportant in the potential range of the LM wave for this system.

(30) For a discussion of the values of pK_a and θ, see later.

Table III. Rate Constants for the Exchange of 4-Methoxy- and 4-Nitropyridines with Various Phosphines N in the 17-Electron Cation Radicals η^5-MeCpMn(CO)$_2$L$^+$ [a]

no.	L	N	log k_1 [b]	pK_a^N [c]	θ [d] (deg)
1	4-MeOpy	P(OMe)Ph$_2$	1.88 (0.03)	2.9[g]	132
9	4-MeOpy	PPhEt$_2$	2.65 (0.04)	6.78	136
10	4-MeOpy	PPh$_2$Et	1.59 (0.03)	4.90	140
11	4-MeOpy	PPh$_3$	0.45 (0.02)	3.04	145
5	4-NO$_2$py	P(OMe)Ph$_2$	2.61 (0.06)	2.9[g]	132
12	4-NO$_2$py	PEt$_3$	4.30 (0.03)	8.65	132
13	4-NO$_2$py	PPhEt$_2$	3.30 (0.04)	6.78	136
14	4-NO$_2$py	PPh$_2$Et	2.23 (0.04)	4.90	140
15	4-NO$_2$py	PPh$_3$	1.22 (0.07)	3.04	145
16	4-NO$_2$py	P(p-MePh)$_3$	1.74 (0.02)	4.41	145[f]
17	4-NO$_2$py	P(p-MeOPh)$_3$	2.18 (0.03)	6.17	145[f]
18	4-NO$_2$py	PPh$_2$Me	3.04 (0.02)	4.65	136
19	4-NO$_2$py	PPh$_2$(n-Bu)	2.14 (0.03)	5.0	141[e]
20	4-NO$_2$py	PPh$_2$(i-Pr)	1.30 (0.15)	5.15	150

[a] In methylene chloride containing ca. 10^{-3} M manganese carbonyl derivative, 10^{-1}–10^{-2} M phosphine, and 0.1 M TBAP at 22 °C. [b] Variance is indicated in parentheses. [c] pK_a^N of the phosphonium/phosphine in water from ref 35–37. [d] Cone angle of the phosphine from ref 40. [e] Estimated value. [f] The value for PPh$_3$ is used, neglecting the effect of the para substituent. [g] Estimated from ref 35 and 36.

of the electronic and steric properties of L and N with the observed rate constant k_1 for ligand substitution in eq 11. Before doing so, however, we must consider some quantitative measures of electronic and steric properties of ligands and nucleophiles.

(I) Electronic and Steric Effects of Pyridine Ligands and Phosphine Nucleophiles. The contribution from the electronic properties of L and N will be evaluated in terms of the pK_a values listed in Tables II and III for the protonated forms of the ligands. The pK_a values relate only to the formation of a pure σ bond (i.e., L–H$^+$ and N–H$^+$), and do not include any back-bonding contribution.[6] Since the magnitude of back-bonding differs with nitrogen-centered and phosphorus-centered ligands, the use of pK_a values allows the entering phosphine nucleophiles and the leaving pyridine ligands to be interrelated via a common σ-basicity scale. Indeed this quantity (or the corresponding difference in the half-neutralization potential ΔHNP[31]) has been frequently used to assess electronic contributions.[32,33] The pK_a values of both pyridines and phosphines with a broad variety of substituents have been measured in water.[31,34,35] [The use of these values in our system is justified by the trend in pK_a values of substituted pyridines, which is known to be the same in water as it is in an aprotic solvent such as acetonitrile.[38]] In order to distinguish the electronic effects of the pyridine ligand and the phosphine nucleophile, they will be designated hereafter as pK_a^L and pK_a^N, respectively.

The steric contributions originating from the pyridine leaving groups are considered to be constant for the para substituents,

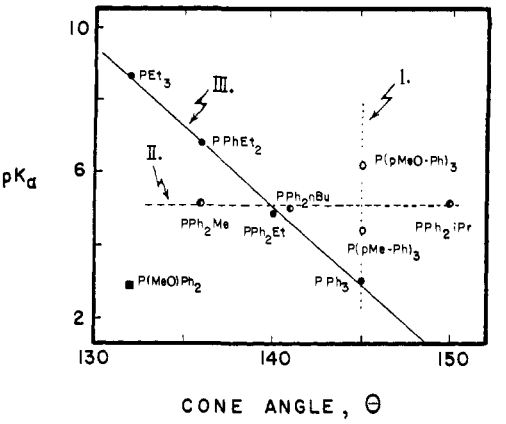

Figure 6. The various relationships between the Tolman cone angle θ and the acid–base dissociative constants [pK_a^N] of phosphine nucleophiles of class I (···), class II (- - -), class III (—), and class IV [P(OMe)Ph$_2$].

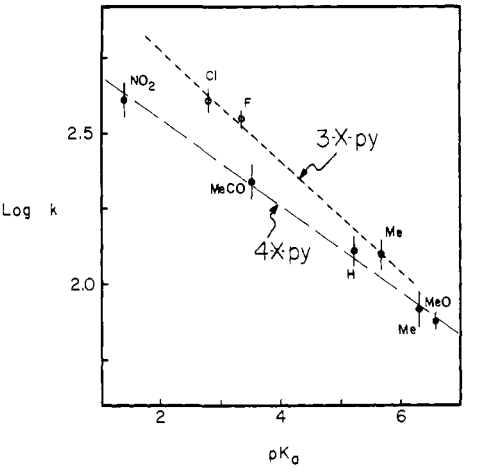

Figure 7. The correlation of the rate constant log k_1 for ligand substitution of MeCpMn(CO)$_2$(py-X)$^+$ with P(OMe)Ph$_2$ and [pK_a^L] of the 3-substituted (- - -) and the 4-substituted (···) pyridine ligands.

as is commonly assumed in the Hammett correlations.[39] Those in the 3-substituted pyridines are likely to be somewhat larger than the para analogues, but not widely variant among themselves owing to their remoteness from the nitrogen center. The steric contributions from the phosphine nucleophiles are usually evaluated by the values of their cone angles θ as defined by Tolman.[40] With this classification in mind, the phosphine nucleophiles considered in this study fall into four general categories. Class I includes the para-substituted triarylphosphines such as triphenylphosphine, tri-p-tolylphosphine, and trianisylphosphine, which are considered to be isosteric. Class II consists of a series of alkyldiphenylphosphines (R–PPh$_2$, where R = methyl, ethyl, n-butyl, and isopropyl), which have roughly the same pK_a^N but differ widely in their cone angles, as shown by the dashed line in Figure 6 (for the phosphines in No. 18, 14, 19, and 20, Table III). Class III phosphines PPh$_n$Et$_{3-n}$ with n = 0, 1, 2, and 3 are those in which the cone angles increase in proportion to their pK_a^N, as shown by the solid line in Figure 6 (for the phosphines in No. 12, 13, 14, and 15, Table III). Class IV represents the remainder of phosphines such as P(OMe)Ph$_2$ which have individual values of pK_a^N and θ.

(II) Structural Effects of Pyridine Leaving Groups and Phosphine Nucleophiles on Ligand Substitution. In order to consider the structural effects of ligands and nucleophiles on reactivity, we can systematically examine three series of ligand substitutions

(31) For phosphines pK_a in water, and ΔHNP, in CH_3NO_2 are linearly related. See, e.g.: Streuli, C. A. *Anal. Chem.* **1960**, *32*, 985.
(32) See, e.g.: Shi, Q.; Richmond, T. G.; Trogler, W. C.; Basolo, F., in press.
(33) See, e.g.: Rerek, M. E.; Basolo, F. *Organometallics* **1983**, *2*, 372.
(34) Fisher, A.; Galloway, W. J.; Vaughan, J. *J. Chem. Soc.* **1964**, 3591.
(35) The [pK_a^L] of a pyridine or phosphine was estimated by the Hammett correlation:[36] [pK_a^L] = 5.32 − 5.80σ or Taft correlation[37] [pK_a^N] = 7.85 − 2.67$\Sigma\sigma^*$.
(36) (a) Henderson, W. A., Jr.; Streuli, C. A. *J. Am. Chem. Soc.* **1960**, *82*, 5791. (b) Gordon, A. J.; Ford, R. A. In "Chemist's Companion"; Wiley: New York, 1972, p 1456; (c) Perrin, D. D.; Dempsey, B.; Serjeant, E. P. "pK_a Prediction from Organic Acids and Bases", Chapman and Hall: New York, 1981.
(37) Taft, R. W., Jr. *J. Phys. Chem.* **1960**, *64*, 1805. Taft, R. W., Jr. In "Steric Effects in Organic Chemistry"; Newman, M. S., Ed.; Wiley: New York, 1956; Chapter 13.
(38) Cauquis, G.; Deronzier, A.; Serve, D.; Vieil, E. *J. Electroanal. Chem.* **1975**, *60*, 205. See also Taagepera et al. (Taagepera, M.; Henderson, W. G.; Brownlee, R. T.; Beauchamp, J. L.; Taft, R. W. *J. Am. Chem. Soc.* **1972**, *94*, 1369) for a comparison of gas-phase and aqueous values of [pK_a^L].
(39) See: Lowry, T. H.; Richardson, K. S. "Mechanism and Theory in Organic Chemistry"; 2nd ed.; Harper and Row: New York, 1981.
(40) Tolman, C. A. *Chem. Rev.* **1977**, *77*, 313. Note that θ is not, strictly speaking, an intrinsic property of the phosphine but depends on the metal–ligand bond considered.

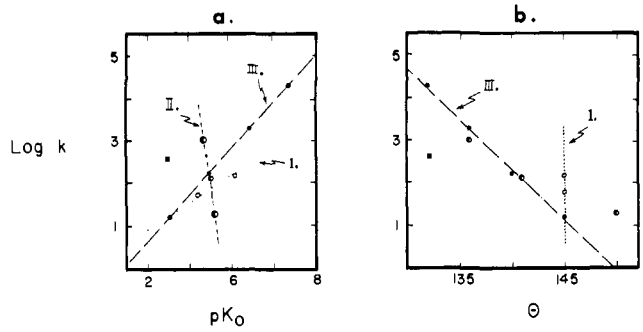

Figure 8. The dependence of the rate constant log k_1 for ligand substitution of $MeCpMn(CO)_2(py\text{-}NO_2)^+$ on $[pK_a^N]$ (left figure) and $[\theta]$ (right figure) of various phosphine nucleophiles N.

consisting of (A) various L toward a common N, (B) common L toward various N, and (C) the general case consisting of various L and N combinations.

(A) The effect of the leaving ligand L on the rate of substitution is reflected in the reactivities of the 3- and 4-substituted pyridine derivatives of $MeCpMn(CO)_2(py\text{-}X)^+$ toward a common nucleophile N = $P(OMe)Ph_2$. The quantitative relationship between the rate of ligand substitution and the pK_a^L of the leaving group L is shown in Figure 7. Although the span of reactivities is somewhat limited, the dependence of the reactivity of a ligand with its electronic properties is unmistakable—the carbonylmanganese cations with pyridine ligands bearing electron-attracting substituents (nitro, acetyl, etc.) being consistently the most reactive. Moreover, two trends are discernible—one for the 4-substituted pyridines and another displaced upwards with a slightly larger slope for the meta derivatives. We are inclined to consider the para series to reflect only electronic effects, since the parent pyridine (X = H) appears to correlate better with it than the meta series. If so, the meta correlation includes a small contribution from steric effects on the leaving group L. The correlation of the data for L = 4-substituted pyridines only can be expressed by the least-squares relationship:

$$\log k_1 = 2.8 - 0.14[pK_a^L] \quad (12)$$

(B) The effect of the entering nucleophile N on the rate of ligand substitution is reflected in the reactivities of various phosphines toward a $MeCpMn(CO)_2L^+$ with a common leaving group such as L = 4-nitropyridine. The range of reactivities in this series is rather large, displaying three orders of magnitude in proceeding from N = triphenylphosphine to triethylphosphine. The effects of the phosphine nucleophile can be initially considered by separating the steric factors (expressed in the cone angle θ) from the electronic factors (expressed by pK_a^N). The results are shown in Figure 8a,b. A cursory examination of these figures reveals no apparent correlation of the reactivity with either pK_a^N or θ. However, a closer scrutiny of the data reveals three separate and unique facets of the reactivity trend for the phosphine nucleophiles. First, for the Class I triarylphosphines with invariant cone angles, the rates increase with base strengths (i.e., pK_a^N, see data points 15, 16, and 17 in Figure 8a). Indeed this trend accords with the results obtained for the variation in the reactivity with pK_a^L of the pyridine ligands in Figure 7. In other words under the conditions of constant steric effect, the rates of ligand substitution increase with electron-attracting substituents on the pyridine ligand L and with electron-releasing substituents on the phosphine nucleophile N. Second, for the Class II phosphines $RPPh_2$ with similar pK_a^N, the ligand substitution rates are shown in Figure 8b (see data points 18, 14, 19, and 20) to decrease with increasing angles, in accord with intuitive expectations of steric hindrance. Third, the Class III phosphines PPh_nEt_{3-n} with $pK_a^N \propto \theta$ show remarkable linear correlations with both pK_a^N and θ in Figure 8, parts a and b, respectively. (See the data points for 12, 14, 13, and 15 identified in Table III.) Furthermore, the slopes of the correlations with pK_a^N and θ follow the trend established for the Class I and II phosphines, respectively. Such a behavior strongly suggests that pK_a^N and θ are not exclusive parameters

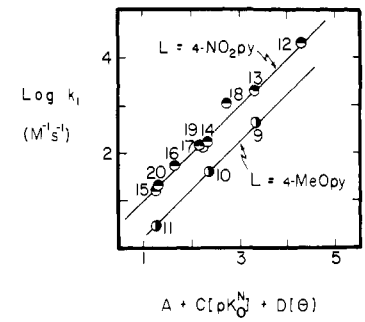

Figure 9. The general correlation of the rate constants log k_1 for ligand substitution of $MeCpMn(CO)_2(py\text{-}NO_2)^+$ (●) and $MeCpMn(CO)_2(py\text{-}OCH_3)^+$ (◑) with the combined steric and electronic effects of the various phosphine nucleophiles according to eq 13 and 14, respectively.

but exert their influence by a linear combination of their individual effects.

This conclusion encouraged us to undertake a linear regression analysis of the data based on a 2-variable dependency (i.e., θ and pK_a^N) of the rate constant k_1. Indeed such an analysis afforded the relationship

$$\log k_1 = 17 + 0.28[pK_a^N] - 0.11[\theta] \quad (13)$$

with a correlation coefficient of 0.98 for all ten phosphine nucleophiles with L = 4-nitropyridine in Table III. Application of the same analysis to L = 4-methoxypyridine yielded

$$\log k_1 = 16 + 0.31[pK_a^N] - 0.11[\theta] \quad (14)$$

Although the latter was evaluated with only a limited number (3) of available data points, the relationship between the two series is clearly evident in the plots in Figure 9, which is in striking contrast to the rather random-looking set of data points in Figure 8b. Both eq 13 and eq 14 can be expressed in the general form

$$\log k_1 = A + C[pK_a^N] + D[\theta] \quad (15)$$

where A, C, and D are constants.

(III) A Unified View of Steric and Electronic Effects on Ligand Substitution. The combined effects of the leaving ligand L and the entering nucleophile N on the rates of ligand substitution are implicit in the two parallel correlations in Figure 9. It follows from this observation that the system consisting of $MeCpMn(CO)_2L^+$ with L = 4-nitropyridine differs from that with L = 4-methoxypyridine by a *constant term*, which presumably arises from both steric and electronic factors in the pyridine leaving group. In order to extract this contribution from the constant term, let us reconsider the empirical relationship in eq 12 in the light of either eq 13 or 14. The linear combination of these separate effects suggests a combined equation of the general form

$$\log k_1 = A + B[pK_a^L] + C[pK_a^N] + D[\theta] \quad (16)$$

[Note the minor variation in the steric effects arising from the pyridine ligand L in Figure 7 is included in the constant A.] In order to test the validity of this general formulation, we performed a 3-variable (i.e., $[pK_a^L]$, $[pK_a^N]$, and $[\theta]$) linear regression analysis of all the systems presented in Tables II and III. The results of the analysis afforded the following relationship

$$\log k_1 = 17 - 0.15[pK_a^L] + 0.28[pK_a^N] - 0.12[\theta] \quad (17)$$

with a correlation coefficient of 0.99 for the 20 systems included. The validity of the general equation obtained by the linear combination of effects is shown by the numerical coefficients in eq 17 which are closely akin for those evaluated in eq 12, 13, and 14 for the separate effects. The agreement between the values of the experimental rate constants and those predicted from eq 17 is illustrated in Figure 10.

The empirical relationship in eq 17 represents a linear free energy relationship for ligand substitution which includes steric and electronic effects for both the leaving ligand L and the entering nucleophile N. As such, the numerical coefficients B, C, and D

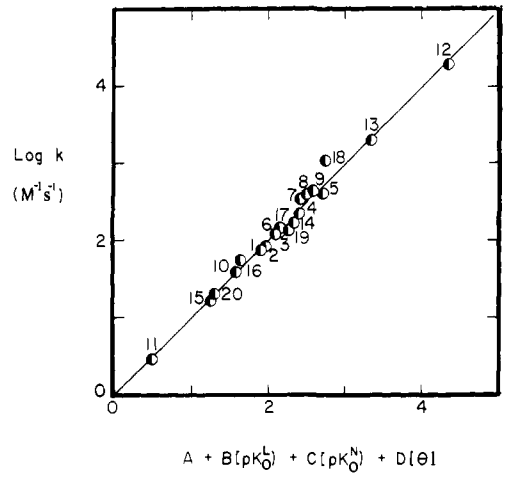

Figure 10. Unified free energy relationship according to eq 17 for the ligand substitution of a series of $MeCpMn(CO)_2(py\text{-}X)^+$ with various phosphine nucleophiles identified by the numbers in Table III.

on the right side of eq 16 (or 17) must bear different units to reflect the energy terms arising from $[pK_a^L]$, $[pK_a^N]$, and $[\theta]$, respectively (including a multiplicative factor of $2.3RT$ for the left side).[41] The absence of cross terms suggests that the coupling between these various contributions is either small or constant and can be incorporated into the coefficient A.[42] [The validity of these types of approximations has been discussed earlier.[43]]

At this juncture we might wonder whether such a free energy relationship can be general for ligand substitution, since we know of no precedent in the extant literature. In somewhat related studies, Trogler, Basolo, and co-workers[32] found that steric contributions were either small or nil in the ligand substitution of the 17-electron $V(CO)_6$ with a variety of phosphine nucleophiles. When their rate data are plotted against the values of pK_a^N for phosphines, a linear relationship results with

$$\log k_1 = -1.6 + 0.42[pK_a^N] \quad (18)$$

The coefficient of 0.4 in eq 18, which compares with a coefficient of 0.3 in eq 13, suggests that the transition states for ligand substitution in $MeCpMn(CO)L^+$ and $V(CO)_6$ are somewhat akin insofar as the entering phosphine nucleophile is concerned. By contrast, the kinetic study by Rerek and Basolo[33] on the 18-electron metal carbonyls η^5-$R_5CpM(CO)_2$, where M = Rh (R = H, Me), Co (R = Me), showed essentially no effect arising from the electronic properties of the phosphine and phosphite ligands. Interestingly, the slopes of the linear correlation of the rates (log k_1) with the cone angles of the phosphine nucleophiles are similar to that presented in eq 13 (or 17).[44]

(IV) Comments on the Transition States for Ligand Substitution. A further comparison of the rates of ligand substitutions in $MeCpMn(CO)_2L^+$ with those observed in $V(CO)_6$ and $Cp'Rh(CO)_2$ is worthwhile. Despite absolute values of k_1 for $MeCpMn(CO)_2L^+$ which are larger by a factor of $\sim 10^3$ than those in $V(CO)_6$, the electronic perturbations by the phosphine nucleophiles are similar in both systems. An analogous comparison of the 18-electron metal carbonyls[33] with the 17-electron radicals reveals rate enhancements by a factor of $\sim 10^7$, which corresponds to a considerable decrease in the activation barrier for ligand exchange.[45] Nonetheless, the degree of phosphine bonding to the metal center in the transition states appears to be similar, judging by their parallel sensitivity to variations in cone angles of the entering nucleophile. The difference may be ascribed to the ability of the Cp ligand in the 18-electron metal carbonyl to accommodate the "20-electron" transition state by converting from η^5 to η^3 ligation (i.e., slippage as suggested by Basolo[46]) and essentially compensate or neutralize the electronic effects of the entering nucleophile. Since such a change is expected to be less necessary in the electron-deficient 17-electron system, the electronic demands would be met by the leaving ligand. The last point is supported by the similar sensitivity of the rates with those in $V(CO)_6$, as indicated by comparison of the C coefficients in eq 13 and 18. We think that the corresponding measurements of the ligand substitution rate constants for the 18-electron precursor, i.e., on $MeCpMn(CO)_2(py)$ itself, will allow a direct test of this formulation.[47]

Various types of mechanisms have been proposed for ligand substitutions in metal carbonyls,[5] which stem from the general classification proposed by Langford and Gray.[48] Accordingly, the ligand substitution step in eq 7 of Scheme I may be considered, in the most general context, as one of the following:

I. Irreversible associative ligand exchange (A_i):

$$L\text{-}M^+ + N \xrightarrow{k} N\text{-}M^+ + L \quad (19)$$

II. Reversible associative ligand exchange (A_r):

$$L\text{-}M^+ + N \underset{k_-}{\overset{k_+}{\rightleftharpoons}} N\text{-}M^+ + L \quad (20)$$

III. Irreversible dissociative ligand exchange (D_i):

$$L\text{-}M^+ \underset{k_-}{\overset{k_+}{\rightleftharpoons}} L + M^+ \text{ (fast)} \quad (21)$$

$$L\text{-}M^+ + N \xrightarrow{k} N\text{-}M^+ \quad (22)$$

IV. Reversible dissociative ligand exchange (D_r):

$$L\text{-}M^+ \underset{k_-}{\overset{k_+}{\rightleftharpoons}} L + M^+ \text{ (fast)} \quad (23)$$

$$M^+ + N \underset{k_-'}{\overset{k_+'}{\rightleftharpoons}} N\text{-}M^+ \quad (24)$$

V. Interchange mechanism (I):

$$L\text{-}M^+ + N \underset{k_-}{\overset{k_+}{\rightleftharpoons}} (L\text{-}M, N)^+ \quad (25)$$

$$(L\text{-}M, N)^+ \xrightarrow{k} (N\text{-}M, L)^+ \quad (26)$$

$$(N\text{-}M, L)^+ \xrightarrow{\text{fast}} N\text{-}M^+ + L \quad (27)$$

The analysis of the electrochemical kinetics associated with each of these mechanisms has been carried out in detail, as described in Table VIII in the Experimental Section. Suffice it to summarize the conclusion at this juncture that the cyclic voltammetric studies typified by the results in Table I and in Figure 2 unequivocally eliminate mechanisms A_r, D_i, and D_r for reasons of molecularity in the substitution step. (For details, see the Experimental Section.) Similarly, the interchange mechanism I can be eliminated when $k_+[N] > k_-$ (see eq 25). The electrochemical kinetics

(41) (a) In the unified free energy relationship, the activation free energy for ligand substitution $\Delta G^\ddagger = -RT \ln k_1$ is considered to be separable into a linear combination of steric (s) and electronic (e) components of L and N such as $\Delta G^\ddagger_{L,e}$, $\Delta G^\ddagger_{L,s}$, $\Delta G^\ddagger_{N,e}$, and $\Delta G^\ddagger_{N,s}$. Other contributions can be included in a term $\Delta G_0^\ddagger$. (b) For example, the steric term for the phosphine should be expressed as $\Delta G^\ddagger_{N,s} \cong k\theta$, where k is the molecular force constant.

(42) The deviation of data points such as No. 18 may be due to such a coupling or to inaccuracies of pK_a and θ measures.

(43) See: Schenkluhm, H.; Berger, H.; Pittel, B.; Zahres, M. *Transition Met. Chem.* **1981**, *6*, 227 and references therein.

(44) The slopes (C) are −0.096 (M = Rh, R = Me), −0.051 (M = Rh, R = H), and −0.102 (M = Co, R = Me) for the displacement of carbon monoxide by phosphines.[33]

(45) For example, the enthalpies of activation for the ligand substitution of the 18-electron metal carbonyls $Cp'M(CO)_2$ average about $\Delta H^\ddagger \cong 15$ kcal mol^{-1}.[33] For the 17-electron $V(CO)_6$ an average of $\Delta H^\ddagger \cong 10$ kcal mol^{-1} is obtained.[32] For $MeCpMn(CO)_2(NCMe)^+$ and PPh_3, $\Delta H^\ddagger = 4.4$ kcal mol^{-1}.[11]

(46) Schuster-Woldan, H. G.; Basolo, F. *J. Am. Chem. Soc.* **1966**, *88*, 1657. See also the discussion in ref 33 and: Casey, C. P.; Jones, W. D. *J. Am. Chem. Soc.* **1980**, *102*, 6156.

(47) Unfortunately such measurements are difficult to carry out reliably owing to the efficiency of the chain process in Scheme I.

(48) Langford, C. H.; Gray, H. B. "Ligand Substitution Processes"; W. A. Benjamin: New York, 1965.

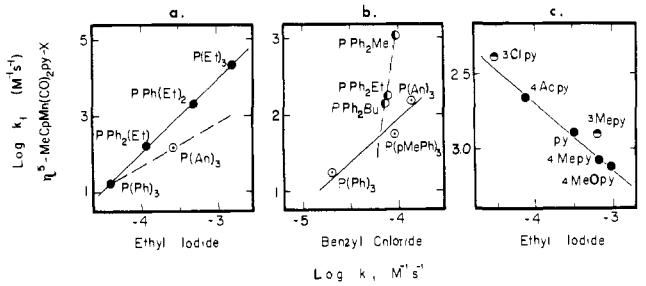

Figure 11. Comparative relationships between ligand substitution on the manganese center and the nucleophilic substitution on carbon centers. (a) Ordinate: log k_1 for MeCpMn(CO)$_2$(pyNO$_2$)$^+$ and PR_3. Abscissa: log k for CH_3CH_2I and PR_3 from ref 51. (b) Ordinate: log k_1 for MeCpMn(CO)$_2$(pyNO$_2$)$^+$ and PR_3. Abscissa: log k for $PhCH_2Cl$ + PR_3 from ref 54. (c) Ordinate: log k_1 for MeCpMn(CO)$_2$(py-X)$^+$ (for 4-X (●) and 3-X (◓)) and P(OMe)Ph$_2$. Abscissa: log k for CH_3CH_2I and py-X from ref 50.

thus leaves us with two alternatives for ligand substitution—the conventional S_N2 or A_j mechanism and the interchange mechanism I (when $k_+[N] \ll k_-$). Since these mechanisms are kinetically indistinguishable, let us reconsider the significance of the coefficients in the unified free energy relationship in eq 16. In particular, we note that the B and C coefficients for $[pK_a^L]$ and $[pK_a^N]$ are similar in eq 17, and of opposite signs as expected for entering group and leaving group effects. The quantitative comparison of these electronic effects must take into account the acid dissociation constants which are not directly related to the strengths of the Mn–L and N–Mn bonds (vide supra). However, their comparable magnitudes do suggest that the transition state binding of pyridine and phosphine is rather symmetrical.[49] If so, it indicates that ligand exchange in MeCpMn(CO)$_2$L$^+$ occurs via a conventional associative S_N2 pathway rather than an interchange mechanism.[52] This formulation is tantamount to a 19-electron transition state about the manganese center during ligand substitution.

Such hypervalent transition states of course have ample analogy in organic chemistry since nucleophilic S_N2 substitution at a tetrahedral carbon center leading to Walden inversion is commonly considered to involve a hypervalent 10-electron trigonal-bipyramidal configuration.[39] As such, it is constructive to compare the reactivities of phosphine nucleophiles acting on the 17-electron manganese center in η^5-MeCpMn(CO)$_2$py$^+$, i.e.,[53]

$$R_3P + Mnpy^+ \rightarrow [R_3PMnpy^+]^\ddagger \rightarrow R_3PMn^+ + py$$

with the same attack on the 8-electron carbon center in organic halides,[51,54] e.g.,

$$R_3P + CH_3CH_2I \rightarrow [R_3PCH_2(CH_3)I]^\ddagger \rightarrow R_3P^+CH_2CH_3 + I^-$$

The correlation of the second-order rate constants for Class III phosphines is shown by the solid line in Figure 11a. The striking linear correlation is expressed by the expression

$$\log k_1^{L\text{-}M} = 9.6 + 1.9 \log k_1^{Et\text{-}I}$$

with a correlation coefficient of 0.99.[55] Such a correlation suggests that nucleophilic attacks on carbon and on manganese respond in the same way to combined steric and electronic effects of the phosphine nucleophile. Essentially the same conclusion is gained from the Class I phosphines (with constant steric effects) shown by the dashed lines in Figure 11, a and b,[56] as it is with the Class II phosphines (with constant electronic effects) shown by the solid line in Figure 11b.[57] Moreover, a comparison of the reactivities of substituted pyridines on manganese and at carbon centers in Figure 11c reflects comparable degrees of bond-making and bond-breaking in the transition states.[58,59]

Summary and Conclusions

Steric and electronic effects on ligand substitutions at metal centers can be successfully probed with a series of structurally related 17-electron carbonylmanganese cations η^5-MeCpMn(CO)$_2$(py-X)$^+$ and various phosphine nucleophiles in eq 1. Advantage from this system accrues from second-order rate constants (log k_1) for ligand substitution which are unusually rapid and strongly subject to steric and electronic effects of both the leaving pyridine ligand (represented by a series of 3- and 4-substituted pyridines py-X) and the entering phosphine nucleophile (represented by various alkyl and aryl phosphines). The electronic effects are evaluated by the acid–base dissociation constants $[pK_a^L]$ and $[pK_a^N]$ of these pyridines and phosphines, respectively. The steric effects of 4-substituted pyridines are taken to be constant (to accord with traditional Hammett correlations), and those of phosphines are evaluated by Tolman's cone angles [θ]. Indeed, the availability of three unique types of phosphines, either with constant steric effects (Class I), constant electronic effects (Class II), or mutually dependent steric and electronic effects (Class III), allows the rates of ligand substitution to be dissected clearly into the three independent parameters $[pK_a^L]$, $[pK_a^N]$, and [θ]. The resulting unified linear free energy relationship expressed by eq 17 with a high correlation coefficient applies to all the experimental data encompassing the various pyridine leaving groups and phosphine nucleophiles, as shown in Figure 10.

Steric and electronic effects in the ligand substitutions of MeCpMn(CO)$_2$(py-X)$^+$ with phosphines are compared to those in related 18-electron rhodium and cobalt carbonyls Cp'M(CO)$_2$ and the 17-electron V(CO)$_6$ which have been recently reported by Basolo, Trogler, and co-workers.[32,33] The reactivities of these 17- and 18-electron metal carbonyls are strongly differentiated by substantial differences in the magnitudes of the activation enthalpies $\Delta H^\ddagger$, but not by differences in the entropies of activation $\Delta S^\ddagger$.

The various types of transition states for ligand substitution as classified by Langford and Gray[48] are also considered. The kinetics analysis of the molecularity in the substitution step as well as the molecular interpretation of the coefficients in the free energy relationship (eq 17) lead to the conclusion that the pyridine leaving group and phosphine nucleophile are more or less equally bonded to the manganese center in the activated complex. Such an associative mechanism for ligand substitution accords with the conventional S_N2 displacement in wholly organic systems. The strong parallel in the steric and electronic effects extant in ligand substitutions at the manganese center and bimolecular nucleophilic substitutions and tetrahedral carbon centers is presented.

The rate constants for the rapid reactions of transient species, such as the labile carbonylmanganese radical cations examined

(49) It is noteworthy that the reactivities (log k) of a series of pyridine and phosphine nucleophiles in their Menschutkin reactions with ethyl iodide follow linear correlations with log $k = -5.9 + 0.49[pK_a^L]$ and log $k = -5.3 + 0.29[pK_a^N]$, respectively.[50,51] The comparable slopes indicate similar degrees of nitrogen and phosphorus bonding in the transition states with these nucleophiles.

(50) Fischer, A.; Galloway, W. J.; Vaughan, J. *J. Chem. Soc.* **1964**, 3596.

(51) (a) Henderson, W. A., Jr.; Buchler, S. A. *J. Am. Chem. Soc.* **1960**, *82*, 5794. (b) Henderson, W. A., Jr.; Streuli, C. A. *Ibid.* **1960**, *82*, 5791.

(52) A geometrically constrained transition state is also indicated by rather large, negative values of the entropy of activation $\Delta S^\ddagger = -25$ eu for MeCpMn(CO)$_2$(NCMe)$^+$ and PPh_3.[11] The ligand substitution of 18-electron metal carbonyls Cp'M(CO)$_2$[33] and the 17-electron V(CO)$_6$[32] also have similar values of $\Delta S^\ddagger = -34$ and -25 eu, respectively.

(53) Stereochemistry at the manganese center is not implied in the example below.

(54) McEwen, W. E.; Jones, A. B.; Knapczyk, J. W.; Kyllingstad, V. L.; Shian, W. I.; Shore, S.; Smith, J. H. *J. Am. Chem. Soc.* **1978**, *100*, 7304.

(55) Data for ethyl iodide substitutions from ref 51.

(56) For the correlations in Figure 11a,b, the slopes are 0.9 and 1.1, respectively. See also footnote 57 in ref 11.

(57) Although the general trends in phosphine reactivities are the same, MeCpMn(CO)$_2$(pyNO$_2$)$^+$ is more sensitive to steric effects than $PhCH_2Cl$, in accord with less steric hindrance expected at the primary carbon center.

(58) By a comparison of our data with that in ref 50.

(59) Although py is a leaving group in MeCoMn(CO)$_2$py and an entering group with ethyl iodide in the Menschutkin reaction, the free energy relationships of the two series should be related. Compare: Arnett, E. M.; Petro, C. *J. Am. Chem. Soc.* **1976**, *98*, 1468.

Table IV. Characterization of the Carbonylmanganese Complexes η^5-MeCpMn(CO)$_2$Y

Y	IR[a] (cm^{-1})	mp[b] (°C)	elemental anal.[c] calcd	found
py	1934, 1868	74–75		
4-CH$_3$Opy	1922, 1855	52–53	C 56.02 H 4.70	C 56.21 H 4.53
4-O$_2$Npy		75–76	C 49.54 H 3.52	C 49.38 H 3.65
4-CH$_3$py	1936, 1870	79–80	C 59.37 H 4.98	C 59.19 H 4.97
4-CH$_3$COpy	1930, 1865	101–101.5	C 51.43 H 3.65	C 51.54 H 3.79
3-CH$_3$py	1935, 1865	62.5–63	C 59.37 H 4.98	C 59.58 H 4.97
3-Fpy		54–55	C 54.38 H 3.86	C 54.40 H 3.93
3-Clpy	1930, 1870	75–76	C 57.84 H 4.53	C 57.55 H 4.82
PEt$_3$	1937, 1874	oil		
P(Me)Ph$_2$	1940, 1878	57–58		
PPh$_3$	1944, 1884	118–119		
P(Et)Ph$_2$	1942, 1884	oil		
P(Et)$_2$Ph	1931, 1868	oil		
P(OMe)Ph$_2$	1944, 1884	65–66		
P(C$_6$H$_4$CH$_3$-p)$_3$	1939, 1879	184–186		
P(C$_6$H$_4$OCH$_3$-p)$_3$	1939, 1878	oil		
P(n-C$_4$H$_9$)Ph$_2$	1939, 1877	oil		
P(i-C$_3$H$_7$)Ph$_2$	1935, 1876	oil		

[a] In n-heptane solution with polystyrene calibration, Perkin-Elmer 298 spectrometer. [b] Uncorrected. [c] Analysis by Galbraith or Midwest Labs.

in this study, can be conveniently carried out with readily available electrochemical instrumentation. The experimental method derives from the electrocatalysis which accompanies the exposure of a series of carbonylmanganese complexes η^5-MeCpMn(CO)$_2$(py-X) to various phosphines. The mechanism of the electrocatalysis in Scheme I is deduced from the effects of the variations in the concentrations of MeCpMn(CO)$_2$(py-X) and phosphine on the cyclic voltammograms recorded at various scan rates. The values of the second-order rate constant (log k_1) for ligand substitution can be extracted by the quantitative analysis of the cyclic voltammograms using Feldberg's computer simulation or Saveant's adimensional analysis of the electrochemical kinetics associated with Scheme I. Both procedures are described in detail in order to encourage their further application to other systems.

Experimental Section

Materials. The substituted pyridines, X-py where X = 4-acetyl, 4-methyl, 3-methyl, 3-chloro, and 3-fluoro, from Aldrich were used without further purification. The 4-methoxy and 4-nitro analogues were prepared by literature methods.[60] Triphenylphosphine (Matheson), triethylphosphine (Pressure Chemical), tri-p-tolylphosphine and trianisylphosphine (M and T Chemical), methyldiphenylphosphine (Organometallics), and methoxydiphenylphosphine (Arapahoe Chemical) were further purified by either distillation or sublimation and stored under argon. Ethyldiphenylphosphine, n-butyldiphenylphosphine, isopropyldiphenylphosphine, and diethylphenylphosphine were prepared from the treatment of either chlorodiphenylphosphine or dichlorophenylphosphine (Alfa) with the appropriate alkylmagnesium bromide.

The carbonylmanganese complexes η^5MeCpMn(CO)$_2$Y listed in Table IV were prepared from η^5-MeCpMn(CO)$_2$(THF) which was generated in situ by the actinic irradiation of a THF solution of η^5-MeCpMn(CO)$_3$ (Alfa) under argon.[11] All preparative reactions were carried out under an atmosphere of argon, and benchtop manipulations utilized Schlenk ware which was flame dried in vacuo to minimize adventitious water. In a typical procedure, a solution of 2.0 g of 9.2 mmol of η^5-MeCpMn(CO)$_3$ in 350 mL of THF was cooled to 0 °C under argon, and it was irradiated with a 100-W medium-pressure Hg lamp until the IR band at 2024 cm^{-1} had diminished to less than 10% of its initial intensity. At this point, 1 equiv (9.2 mmol) of Y = py (pyridine), 3-Mepy, 4-Mepy, 3-Clpy, 3-Fpy, 4-CH$_3$COpy, 4-CH$_3$Opy, 4-O$_2$Npy, MePPh$_2$, PPh$_3$, (p-CH$_3$C$_6$H$_4$)$_3$P, Et$_3$P, (p-CH$_3$OC$_6$H$_4$)$_3$P, n-BuPPh$_2$, i-PrPPh$_2$, or Et$_2$PPh was added, and the solution stirred at room temperature for up to 12 h. Removal of the THF under vacuo afforded the solid product which was redissolved in ether, and then filtered under argon. Addition of hexane followed by cooling afforded η^5-MeCpMn(CO)$_2$Y in 30–70% yields, and they were further purified by Florisil chromatography and/or recrystallization under argon.[61]

Table V. Standard Oxidation Potentials of MeCpMn(CO)$_2$Y Derivatives with Y = 3- and 4-Substituted Pyridines and Various Phosphines[a]

Y	E^0 (V vs. SCE)	ΔE_p[b] (mV)
pyridine	0.09	67
4-MeOpy	0.04$_5$	81
4-Mepy	0.06	74
4-CH$_3$COpy	0.12$_5$	56
4-NO$_2$py	0.19	101
3-Mepy	0.07$_5$	61
3-Fpy	0.15	73
3-Clpy	0.13$_5$	63
P(OMe)Ph$_2$	0.58	84
PEt$_3$	0.39	101
PPhEt$_2$	0.42$_5$	126
PPh$_2$Et	0.46	72
PPh$_2$Me	0.46$_5$	89
PPh$_2$(n-Bu)	0.45$_5$	104
PPh$_3$	0.49	88
P(C$_6$H$_4$CH$_3$p)$_3$	0.50	85
P(C$_6$H$_4$OCH$_3$-p)$_3$	0.41	104

[a] In CH$_2$Cl$_2$ containing 0.1 M TBAP at 22 °C with a platinum working electrode. [b] At 0.5 V s^{-1}.

Tetra-n-butylammonium perchlorate (TBAP, G. F. S. Smith Chemical) was recrystallized twice from a mixture of ethyl acetate and isooctane and dried in vacuo. n-Hexane and diethyl ether (analytical reagent, Mallinckrodt) were distilled from sodium benzophenone and stored in a Schlenk flask under argon. Methylene chloride (analytic reagent, Mallinckrodt) was initially stirred with concentrated sulfuric acid and then separated, neutralized, and dried over anhydrous Na_2CO_3. It was finally distilled from freshly pulverized calcium hydride under argon. A 1-L three-compartmental cell for bulk electrolysis consisted of a large Pt gauze working electrode (ca. 100 cm^2), a nichrome counter electrode, and a salt bridge. The cell was flame dried in vacuo, refilled with argon, and charged with 0.1 mol of tetra-n-butylammonium perchlorate. The purified CH_2Cl_2 (1 L) was transferred with the aid of a cannula to the cell, and the solution was reduced at a constant potential of −0.5 V vs. SCE until the current fell to <2 μA. The resulting electrolyte was transferred with the aid of a cannula to a Schlenk flask and degassed via three consecutive freeze–pump–thaw cycles to remove the last traces of oxygen.

Electrochemical Measurements. Since the various substituted pyridine analogues of η^5-MeCpMn(CO)$_2$py are photosensitive,[62] all manipulations were carried out in a light-tight dark box, and special precautions were taken to avoid contamination by moisture.

Electrochemistry was performed with an IR-compensated potentiostat[63] driven by a Princeton Applied Research Model 175 universal programmer. The high impedance voltage follower amplifier was mounted external to the potentiostat to minimize the length of the connection to the reference electrode for low noise pickup. Cyclic voltammetric curves were either displayed on a Tetronix 5115 storage oscilloscope or recorded on a Houston Series 2000 X–Y recorder. The magnitude of the anodic peak current was determined by direct examination of the oscilloscope display using a 1-mm resolution grid. The current axis was amplified via the potentiostat sensitivity to optimize signal to noise in measuring the peak current. The pollution of the electrode was not a problem provided the potential was not allowed to become more positive than 1.2 V vs. SCE. The aging of the solution was also not a problem under these conditions since we were able to reproduce the potential/current profiles throughout the course of an experiment. The working electrode was periodically polished with a very fine emery cloth.

The cyclic voltammetric cell was of air-tight design with high-vacuum Teflon valves and viton O-ring seals to allow an inert atmosphere to be maintained without contamination by grease. The adjustable platinum working electrode was imbedded in a cobalt glass seal to allow periodic

(60) Ochiai, E. *J. Org. Chem.* **1953**, *18*, 534.

(61) Connelly, N. G.; Kitchen, M. D. *J. Chem. Soc., Dalton Trans.* **1977**, 931.

(62) Giordana, P. J.; Wrighton, M. S. *Inorg. Chem.* **1977**, *16*, 160.

(63) (a) Garreau, D.; Savêant, J.-M. *J. Electroanal. Chem.* **1972**, *35*, 309. (b) Garreau, D.; Savêant, J.-M. *Ibid.* **1974**, *50*, 22.

Table VI. Experimental Variation of the Peak Current Ratio with Scan Rate in the Cyclic Voltammograms for a Representative Run[a]

run[a] v ($V\ s^{-1}$)	$i_{p'}^0$ (μA)	i_p (μA)	$i_p/i_{p'}^0$	i_p/i_p^0	log $([N]RT/\mathcal{F}v)$
100	59.2	32.0[b]	0.540	1.01	−4.83
50	44.8	24.0[b]	0.536	1.00	-4.52_5
20	30.4	16.0[b]	0.526	0.98_5	−4.13
10	23.2	12.4[b]	0.534	1.00	−3.83
5	16.8	8.80	0.524	0.98	-3.52_5
2	11.2	5.44	0.486	0.91	−3.13
1	8.00	3.52	0.440	0.82_5	−2.83
0.5	6.08	2.24	0.368	0.69	-2.52_5
0.2	3.84	0.96	0.250	0.47	−2.13
0.1	2.80	0.40	0.143	0.27	−1.83

[a] For 8×10^{-4} M η^5-MeCpMn(CO)$_2$(py-Ac-4) and 6×10^{-2} M P(OMe)Ph$_2$ in CH_2Cl_2 containing 0.1 M TBAP at 22 °C. [b] At these scan rates the CV consisted only of the reversible L-M wave (and no CV wave for N-M).

polishing without significantly changing the surface area of approximately 1 mm^2. The SCE reference and saturated KCl salt bridge were separated from the solution by a cracked glass tip. The counter electrode, consisting of a platinum gauze, was separated from the working electrode by less than 2 mm and connected to the reference electrode via a 0.1 μF capacitor to aid in the compensation for IR drop.

In a typical procedure, a 25-mL volumetric flask fitted with a high-vacuum Teflon stopcock was flame dried in vacuo and then charged with 2×10^{-5} mol of η^5-MeCpMn(CO)$_2$py and 25 mL of 0.1 M TBAP in CH_2Cl_2. A 5-mL aliquot was transferred with the aid of a hypodermic syringe to the dry cyclic voltammetric cell in the dark and under an argon atmosphere. The cyclic voltammograms were obtained at a variety of scan rates. (The solution was stirred magnetically after each CV scan.) An aliquot of the phosphine nucleophile was added and the procedure repeated.

The standard oxidation potentials of the reactant MeCpMn(CO)$_2$(py-X) and of the product MeCpMn(CO)$_2$PR$_3$ were evaluated from the anodic and cathodic peak potentials E_P^a and E_P^c, respectively, of the reversible cyclic voltammograms which showed the peak current ratios i_p^a/i_p^c to be consistently close to one at $v \geq 0.1$ V s^{-1}. The values of $E^0 = (E_p^a + E_p^c)/2$, calibrated relative to a ferrocene standard,[64] are given in Table V.

The current function $i_{p'}^0$ relating the peak current of η^5-MeCpMn(CO)$_2$py = LM in the absence of phosphine nucleophile was initially measured independently as a function of the scan rate v. For a reversible fast electron transfer, a linear dependence with $v^{1/2}$ is expected. Since the rate of electron transfer with η^5-MeCpMn(CO)$_2$py is not very fast, however, we observed a slightly bent function $i_{p'}^0$.[65] The peak current function i_p for L−M in the presence of a given concentration of phosphine N was then also recorded as a function of v. The quotient $i_p/i_{p'}^0$ is proportional to the experimental peak current ratio, defined in the text, i.e., $i_p/i_{p'}^0 = \alpha(i_p/i_p^0)$. The proportionality constant α for the run depends on $[L-M_0]$ and S the area of the electrode. It is given by $\alpha = ([L-M_0]S)/(L-M_0]S_0')$. The value of α can be gained by noting that $i_p/i_{p'}^0$ approached unity as v increased (see Figure 12). Thus, experimentally $i_p/i_{p'}^0$ attained a limiting value (i.e., α) for $v > 5$–10 V s^{-1}. [It was checked that when $i_p/i_{p'}^0$ reached its plateau value, the cyclic voltammogram corresponded to no product N−M being formed and a reversible CV for the reactant L−M. This provided additional proof that the value of v considered was sufficient to avoid any significant substitution of L−M$^+$.] Normalization of $i_p/i_{p'}^0$ with respect to α afforded the peak current ratio i_p/i_p^0. The results of a typical run are given in column 5 of Table VI for the electrocatalytic ligand substitution of η^5-MeCpMn(CO)$_2$(py-Ac-4)$^+$ by P(OMe)Ph$_2$ as previously described in Figure 4b. For this particular run, α was found to be 0.534 by averaging the values of $i_p/i_{p'}^0$ at $v \geq 10$ V s^{-1}.

The peak current ratio i_p/i_p^0 obtained by the procedure described above was plotted against the experimental parameter log $([N]RT/\mathcal{F}v)$ for all the runs corresponding to variations in [L−M], [N], and v. The agreement of the experimental data with the theoretical working curve (see Figure 4) was first generally recognized by overlapping the experimental points on the theoretical working curve by sliding it along the abscissa so that the two scales $(i_p/i_p^0)_{expt}$ and $(i_p/i_p^0)_{theor}$ matched. When the best visual fit was achieved the value of log λ corresponding to the origin of the experimental curve was taken as the estimate of log k_1. In order to obtain a statistically averaged value of log k_1, the value of log λ was determined from the working curve for each value of i_p/i_p^0. Subtraction from the experimental log $([N]RT/\mathcal{F}v)$ afforded log k_1 for a particular value of i_p/i_p^0. This procedure was repeated for each value of i_p/i_p^0 corresponding to different [L−M], v, and [N]. For the statistical treatment of the data, only those values of $i_p/i_p^0 < 0.9$ were used. The treatment of the data for larger values of i_p/i_p^0 involves larger errors owing to its asymptotic behavior. We estimate from the reproducibility that the absolute error in i_p/i_p^0 is $\sim\pm0.05$, leading to a random error of ±0.6 in log k_1 when $i_p/i_p^0 \cong 0.9$, ±0.3 when $i_p/i_p^0 \cong 0.8$, and ±0.20 when $i_p/i_p^0 \cong 0.5$. A typical result is given in Table VII.

Table VII. Determination of the Rate Constant (log k_2) for a Typical Run for Ligand Substitution[a]

i_p/i_p^0	log $([N]RT/\mathcal{F}v)_{expt}$	log λ	log k_2 ($M\ s^{-1}$)	
0.82_5	−2.83	−0.707	2.12	2.18 ± 0.07[b]
0.69	-2.52_5	−0.375	2.15	
0.47	−2.13	$+0.037_5$	2.17	
0.27	−1.83	+0.437	2.27	

[a] For 8×10^{-4} M η^5-MeCpMn(CO)$_2$(py-Ac-4) and 6×10^{-2} M P(OMe)Ph$_2$ in CH_2Cl_2 containing 0.1 M TBAP at 22 °C. [b] Average of numbers in column 4. Note that the value (2.34 ± 0.06) given in Table II was obtained from the statistical treatment of all the data presented in Table I.

Evaluation of the Rate Constant k_1 from the Computer Simulation of the Cyclic Voltammogram. The simulation procedure consists of the transcription of the differential eq 28–32 and the boundary conditions applicable to the mechanism in Scheme I into finite difference forms,[15] where [C] is the concentration of species C at time t and distance x from the electrode and D_C is the diffusion coefficient of species C.

$$\partial[L-M]/\partial t = D_{L-M}(\partial^2[L-M]/\partial x^2) - k_2[N-M^+][L-M] \quad (28)$$

$$\partial[L-M^+]/\partial t = D_{L-M^+}(\partial^2[L-M^+]/\partial x^2) - k_1[L-M^+][N] + k_2[N-M^+][L-M] \quad (29)$$

$$\partial[N-M^+]/\partial t = D_{N-M^+}(\partial^2[N-M^+]/\partial x^2) + k_1[L-M^+][N] - k_2[N-M^+][L-M] \quad (30)$$

$$\partial[N-M]/\partial t = D_{N-M}(\partial^2[N-M]/\partial x^2) + k_2[N-M^+][L-M] \quad (31)$$

$$\partial[N]/\partial t = D_N(\partial^2[N]/\partial x^2) - k_1[L-M^+][N] \quad (32)$$

Examination of eq 28–32 shows that the variation of [C] at a given time and location in the diffusion layer is given by two types of terms: the first, $D_C(\partial^2[C]/\partial x^2)$, represents the effect of mass transport arising exclusively from a diffusional origin, and the second represents the effect of the changes in [C] owing to its chemical production (positive term) or chemical destruction (negative term), i.e.,

$$\partial[C]/\partial t = (\partial[C]/\partial t)_{diff} + (\partial[C]/\partial t)_{c.p.} - (\partial[C]/\partial t)_{c.d.} \quad (33)$$

Owing to the nonlinear coupling terms it is seen (even without a consideration of the boundary conditions) that no general mathematical solution exists for this set of differential equations in terms of concentration changes with t and x. Thus the complete solution of the problem utilizes a numerical procedure which requires the direct transcription of eq 28–32 into a finite element form and the resolution of the linear system so obtained by known numerical procedures.[66] Basically the time and space are divided into small elements Δt and Δx, respectively. The concentration of species C at time $t = k\Delta t$ and space $x = j\Delta x$ is expressed as $[C]_{k,j}$. The finite transcription of the various operators is

$$(\partial[C]/\partial t)_{t,x} \cong ([C]_{k+1,j} - [C]_{k,j})/\Delta t \quad (34)$$

$$(\partial^2[C]/\partial x^2)_{t,x} \cong ([C]_{k,j-1} - 2[C]_{k,j} + [C]_{k,j+1})/\Delta x^2 \quad (35)$$

(64) Gagne, R. R.; Koval, C. A.; Lisensky, G. C. *Inorg. Chem.* **1980**, *19*, 2854.

(65) See, e.g. Nadjo, L.; Savéant, J.-M. *J. Electroanal. Chem.* **1973**, *48*, 113.

(66) (a) Crank, J. In "Mathematics of Diffusion"; Oxford at the Clarendon Press: London, 1964. (b) Smith, G. D. In "Numerical Solution of Partial Differential Equations"; Oxford University Press: London, 1971.

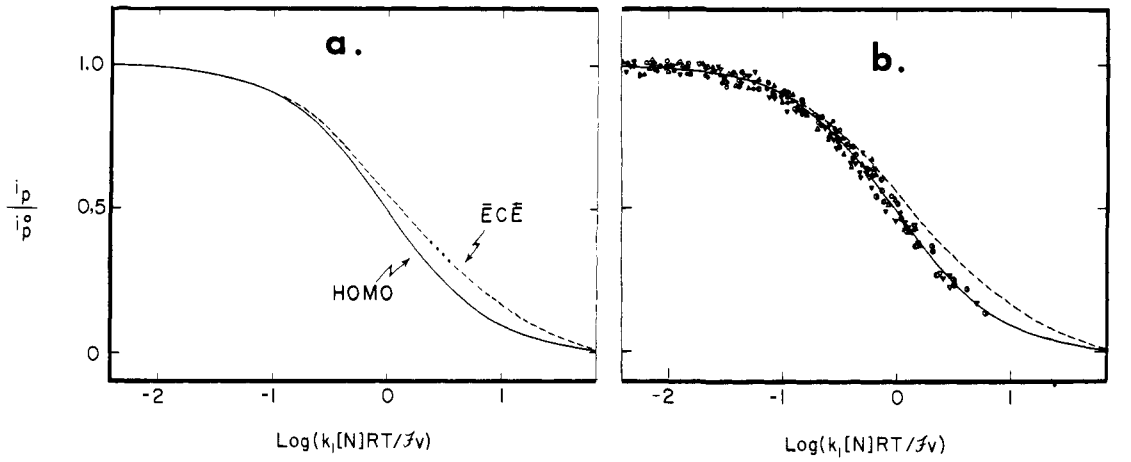

Figure 12. (a) The calculated working curves for the ĒCĒ (---) and HOMO (—) mechanisms applicable to Scheme I. (b) The experimental data points shown in relation to the ECE and HOMO mechanisms.

at $t = k\Delta t$ and $x = j\Delta x$. Thus the set of differential equations applicable to Scheme I can be reexpressed as

$$[\text{L-M}]_{k+1,j} = [\text{L-M}]_{kj} + \{D_{\text{L-M}}(\Delta t/\Delta x^2)\}\{[\text{L-M}]_{kj-1} - 2[\text{L-M}]_{kj} + [\text{L-M}]_{kj+1}\} - (k_2\Delta t)[\text{N-M}^+]_{kj}[\text{L-M}]_{kj} \quad (36)$$

$$[\text{L-M}^+]_{k+1,j} = [\text{L-M}^+]_{kj} + \{D_{\text{L-M}^+}(\Delta t/\Delta x^2)\}\{[\text{L-M}^+]_{kj-1} - 2[\text{L-M}^+]_{kj} + [\text{L-M}^+]_{kj+1}\} - (k_1\Delta t)[\text{L-M}^+]_{kj}[\text{N}]_{kj} + (k_2\Delta t)[\text{N-M}^+]_{kj}[\text{L-M}]_{kj} \quad (37)$$

$$[\text{N-M}^+]_{k+1,j} = [\text{N-M}^+]_{kj} + \{D_{\text{N-M}^+}(\Delta t/\Delta x^2)\}\{[\text{N-M}^+]_{kj-1} - 2[\text{N-M}^+]_{kj} + [\text{N-M}^+]_{kj+1}\} + (k_1\Delta t)[\text{L-M}^+]_{kj}[\text{N}]_{kj} - (k_2\Delta t)[\text{N-M}^+]_{kj}[\text{L-M}]_{kj} \quad (38)$$

$$[\text{N-M}]_{k+1,j} = [\text{N-M}]_{kj} + \{D_{\text{L-M}}(\Delta t/\Delta x^2)\}\{[\text{N-M}]_{kj-1} - 2[\text{N-M}]_{kj} + [\text{N-M}]_{kj+1}\} + (k_2\Delta t)[\text{N-M}^+]_{kj}[\text{L-M}]_{kj} \quad (39)$$

$$[\text{N}]_{k+1,j} = [\text{N}]_{kj} + \{D_{\text{N}}(\Delta t/\Delta x^2)\}\{[\text{N}]_{kj-1} - 2[\text{N}]_{kj} + [\text{N}]_{kj+1}\} - (k_1\Delta t)[\text{L-M}^+]_{kj}[\text{N}]_{kj} \quad (40)$$

If the set of $[\text{C}]_{kj}$ is known for all the species L-M, N-M$^+$, etc., at time $t = k\Delta t$ for all distances $x = j\Delta x$ from the electrode, then their concentration at time $t + \Delta t = (k + 1)\Delta t$ is determined by eq 36-40 for all distances except $j = 0$ and $j = j_{max}$. [Note j_{max} is the index defined by $x_{max}/\Delta x$ where x_{max} is the maximum distance from the electrode reached by the electrochemical perturbation.] The values of $[\text{C}]_{k+1,0}$ are given by the solution of the set of boundary conditions expressing the electrochemical perturbation of the interface between the electrode and the medium. The values of $[\text{C}]_{k+1,j_{max}}$ are identical with those at the initial concentration at $t = 0$, since the solution remains unchanged from $x \geq x_{max}$. This procedure allows the concentration of all species [L-M, L-M$^+$, N-M, N-M$^+$, and N] to be evaluated at any time for any distance from the electrode given the initial conditions at $t = 0$. Since the current flowing through the electrode at a given time is

$$i = -\mathcal{F}S\{D_{\text{L-M}}(\partial[\text{L-M}]/\partial x)_{x=0} + D_{\text{N-M}}(\partial[\text{N-M}]/\partial x)_{x=0}\} \quad (41)$$

where S is the surface area of the electrode, in finite differences the current is

$$i_k = -(\mathcal{F}S/\Delta x) \times \{D_{\text{L-M}}([\text{L-M}]_{k,1} - [\text{L-M}]_{k,0}) + D_{\text{N-M}}([\text{N-M}]_{k,1} - [\text{N-M}]_{k,0})\} \quad (42)$$

From the computed values of [L-M] and [N-M] according to eq 36 and 39, the current is calculated from eq 42 at any given time to afford the current vs. time function for the production of the simulated CV.

Evaluation of the Rate Constant k_1 by the Method of Adimensional Analysis. According to Saveant, the set of partial differential eq 28-32 are recast in an adimensional form using the following parameters:

Concentration variables

$$a = [\text{L-M}]/[\text{L-M}_0], \qquad b = [\text{L-M}^+]/[\text{L-M}_0], \qquad c = [\text{N-M}^+]/[\text{L-M}_0]$$

where $[\text{L-M}_0]$ is the initial concentration. In the following, we restrict ourselves to the CV wave of L-M with N in excess.

Time variable

$$\tau = t[\mathcal{F}v/RT]$$

Space variable

$$y = x[\mathcal{F}v/DRT]^{1/2}$$

where D is the average diffusion coefficient.

Rate constant

$$\text{pseudo first order} \quad \lambda_1 = k_1[\text{N}][RT/\mathcal{F}v]$$

$$\text{second order} \quad \lambda_2 = k_2[\text{L-M}_0][RT/\mathcal{F}v]$$

Potential variable

$$\xi = [\mathcal{F}/RT][E - E_R^0]$$

where E is the electrode potential. With these notations, the kinetics of the mechanism in Scheme I is reduced to

$$\partial a/\partial\tau = \partial^2 a/\partial y^2 - \lambda_2 ac \quad (43)$$

$$\partial b/\partial\tau = \partial^2 b/\partial y^2 - \lambda_1 b + \lambda_2 ac \quad (44)$$

$$\partial c/\partial\tau = \partial^2 c/\partial y^2 + \lambda_1 b - \lambda_2 ac \quad (45)$$

and the boundary conditions for fast electron transfer are[67]

$$\tau = 0,\ a = 1,\ b = c = 0 \text{ for any } y \quad (46)$$

$$\tau > 0,\ y = 0 \quad (47)$$

$$\partial a/\partial y + \partial b/\partial y = 0;\ c = 0;\ a_0 = b_0 \exp(-\xi)$$

$$\tau > 0,\ y \to \infty \quad (48)$$

$$a \to 1,\ b \text{ and } c \to 0$$

The current flowing through the electrode is given by

$$\Psi = -(\partial a/\partial y)_{x=0} + (\partial c/\partial y)_{x=0}$$

where $\Psi = i/\{\mathcal{F}S[\text{L-M}_0][D\mathcal{F}v/RT]^{1/2}\}$. According to this formulation, the system depends only on the magnitudes of the adimensional rate constants λ_1 and λ_2, which encompass the effects of all the dimensional experimental variables of importance here.

Let us now consider in more detail the role of λ_1 and λ_2 in determining the contribution from electron transfer in eq 8 of Scheme I. Two limiting situations will arise according to the magnitude of the ratio λ_2/λ_1, i.e., $(k_2/k_1)([\text{L-M}_0]/[\text{N}])$.

(i) When λ_2/λ_1 is small the term $\lambda_2 ac$ will be negligible compared to $\lambda_1 b$, and eq 43-45 simplify to

$$\partial a/\partial\tau = \partial^2 a/\partial y^2 \quad (49)$$

$$\partial b/\partial\tau = \partial^2 b/\partial y^2 - \lambda_1 b \quad (50)$$

$$\partial c/\partial\tau = \partial^2 c/\partial y^2 + \lambda_1 b \quad (51)$$

(67) The cyclic voltammograms of $MeCpMn(CO)_2py$ are actually indicative of quasireversible electron transfer since ΔE_p in Table V are larger than 60 mV.[68] However, the values of i_p/i_p^0 are only affected slightly by k_1 (see ref 11), and the error is minor.

Table VIII. Chemical Kinetics Terms for the Mechanistic Categories for Ligand Substitution According to Langford and Gray[48]

designated mechanism[a]	$\partial[\text{L-M}^+]/\partial t$[b]	adimensional parameteric form[c]
A_i	$-k[\text{L-M}^+][\text{N}]$	$k(RT/\mathcal{F}v)[\text{N}]$
A_r	$-k_+[\text{L-M}^+][\text{N}] + k_-[\text{N-M}^+][\text{L}]$	$\begin{cases} k_+(RT/\mathcal{F}v)[\text{N}] \\ k_+/k_-)([\text{N}]/[\text{L-M}_0]) \end{cases}$
D_i[d]	$-\dfrac{kk_+[\text{L-M}^+][\text{N}]}{k[\text{N}] + k_-[\text{L}]}$	$\begin{cases} k_+(RT/\mathcal{F}v) \\ (k/k_-)([\text{N}]/[\text{L-M}_0]) \end{cases}$
D_r[d]	$-\dfrac{k_+k_+'[\text{L-M}^+][\text{N}] - k_-k_-'[\text{N-M}^+][\text{L}]}{k_-[\text{L}] + k_+'[\text{N}]}$	$\begin{cases} k_+(RT/\mathcal{F}v) \\ (k_+'/k_-)[\text{N}]/[\text{L-M}_0] \\ k_-'(RT/\mathcal{F}v) \end{cases}$
I[e]	$-\dfrac{kk_+}{k + k_-}[\text{L-M}^+][\text{N}]$	$[kk_+/(k + k_-)](RT/\mathcal{F}v)[\text{N}]$
I[f]	$-\dfrac{k(k_+/k_-)[\text{L-M}^+][\text{N}]}{1 + (k_+/k_-)[\text{N}]}$	$\begin{cases} k(RT/\mathcal{F}v) \\ (k_+/k_-)[\text{N}] \end{cases}$

[a] The subscripts i and r refer to overall irreversibility or reversibility, respectively, of the ligand substitution. [b] Changes in concentration arising only from substitution reactions. [c] For a solution containing excess N and no L; $[\text{L-M}_0]$ is the concentration of L-M initially. If L is initially present in excess $[\text{L-M}_0]$ should be replaced by [L] in the expressions of the adimensional parameters. [d] $[\text{M}^+]$ in the steady state. [e] $[\text{L-M, N}]^+$ and $[\text{N-M, L}]^+$ in steady state. [f] $[\text{N-M}^+, \text{L}]^+$ in the steady state and $[\text{L-M, N}]^+$ in equilibrium, i.e., for $k << k_-$.

In dimensional terms, this means that only a small fraction of N-M^+ generated in eq 7 ($\lambda_1 b$) is reduced in eq 8 ($\lambda_2 ac$). This limiting situation can thus be described as an electrochemical ĒCĒ mechanism.

(ii) When λ_2/λ_1 is large, $[\text{N-M}^+]$ will reach a steady state, i.e., $\lambda_2 ac \cong \lambda_1 b$, since N-M^+ cannot be consumed faster than it is produced. The kinetics thus reduce to the following form:

$$\partial a/\partial \tau = \partial^2 a/\partial y^2 - \lambda_1 b \tag{52}$$

$$\partial b/\partial \tau = \partial^2 b/\partial y^2 \tag{53}$$

$$c \cong 0 \tag{54}$$

In other words N-M^+ is reduced only by homogeneous electron transfer in eq 8, and the contribution from heterogeneous electron transfer in eq 9 is negligible. This limiting situation requires no input from the electrode and is a purely homogeneous catalytic process, which we describe as a HOMO mechanism.

It is important to recognize that in both limiting situations the kinetics depend only on λ_1 which is therefore the unique parameter of significance in this system. The electrochemical kinetics of the ĒCĒ and HOMO mechanisms can be solved by the same numerical approach described for the simulation procedure above to afford the variations of the current ratios $i_p(\lambda_1)/i_p(\lambda_1 = 0) = i_p/i_p^0$, with λ_1. The results are illustrated in Figure 12a for the ĒCĒ and HOMO mechanisms as the solid and dashed lines, respectively. All the experimental data in this study are included by the data points in Figure 12b which is clearly not consistent with a pure ĒCĒ mechanism for ligand substitution. For intermediate values of λ_2/λ_1, the same treatment based on eq 43–45 generates a series of working curves which fall between the two limiting situations described as ĒCĒ and HOMO.

Mechanistic Formulations of the Ligand Substitution Step. Let us now reformulate the mechanism in Scheme I in a more general form in which the ligand substitution step in eq 7 differs somewhat. Such a less restrictive formulation relates to a more general approach in classifying ligand exchange processes according to Langford and Gray[48] in terms of associative (A), dissociative (D), and interchange (I) mechanisms in eq 19–27 (where the subscripts i and r will refer to irreversible and reversible processes, respectively).

The method of adimensional analysis is very well suited to be used to develop a kinetic criterion to examine these mechanistic possibilities. For the sake of clarity, we will only focus on the two limiting situations described above in which the homogeneous electron-transfer step in eq 8 contributes either 0% or 100%, corresponding to the ĒCĒ and HOMO mechanisms, respectively. Thus, let us reconsider the ligand substitution in eq 7 as reversible and the kinetics in both directions describable by an overall term §, i.e.

$$\partial[\text{L-M}^+]/\partial t = -\S \tag{55}$$

$$\partial[\text{N-M}^+]/\partial t = +\S \tag{56}$$

(i) For the ĒCĒ mechanism, we obtain by application of the above procedure

$$\partial a/\partial \tau = \partial^2 a/\partial y^2 \tag{57}$$

$$\partial b/\partial \tau = \partial^2 b/\partial y^2 - \Lambda \tag{58}$$

$$\partial c/\partial \tau = \partial^2 c/\partial y^2 + \Lambda \tag{59}$$

where the adimensional parameter $\Lambda = \S(RT/\mathcal{F}v[\text{L-M}_0])$. Note the boundary conditions are unchanged from that given in eq 46–48.

(ii) For the HOMO mechanism (as presented in eq 52–54), $[\text{N-M}^+]$ exhibits steady state behavior, and the corresponding set of partial differential equations is

$$\partial a/\partial \tau = \partial^2 a/\partial y^2 - \Lambda \tag{60}$$

$$\partial b/\partial \tau = \partial^2 b/\partial y^2 \tag{61}$$

$$c \cong 0 \tag{62}$$

with the boundary conditions set by eq 46–48.

In both of the limiting conditions (i.e., eq 57–59 and eq 60–62), the kinetic behavior is determined only by the magnitude of a single adimensional term Λ, which includes the effects of all the experimental variables of interest to us. Accordingly, let us express Λ, and therefore §, for the various types of mechanisms designated in eq 19–27 for the ligand substitution of L-M^+. (Hereafter we will consider the phosphine nucleophile [N] to be in excess and no free pyridine ligand [L] to be available initially. The adimensional concentration of L is designated as l and defined in the usual form as $l = [\text{L}]/[\text{L-M}_0]$.) The results are summarized in Table VIII and their derivations described briefly below.

For mechanism A_i, eq 7 in Scheme I is the actual elementary step defined as $\S = k[\text{N}][\text{L-M}^+]$ and leading to $\Lambda = k[\text{N}][RT/\mathcal{F}v]b$. The kinetic behavior of this system depends on only a single parameter, $\Lambda = k[\text{N}][RT/\mathcal{F}v]$. For mechanism A_r, the kinetic term is $\S = k_+[\text{L-M}^+][\text{N}] - k_-[\text{N-M}^+][\text{L}]$, leading to $\Lambda = \{k_+[\text{N}](RT/\mathcal{F}v)\}\{b - (k_-/k_+)([\text{N}]/[\text{L-M}_0])cl\}$. The observed kinetics thus depend on two adimensional parameters, $\lambda = k_+[\text{N}][RT/\mathcal{F}v]$ and $\mu = (k_+/k_-)([\text{N}]/[\text{L-M}_0])$. For mechanism D_i, $[\text{M}^+]$ is in the steady state owing to reversibility in the CV wave of L-M in the absence of N. Thus $[\text{M}^+] = k_+[\text{L-M}^+]/(k_-[\text{L}] + k[\text{N}])$ leading to $\S = kk_+[\text{N}][\text{L-M}^+]/(k_-[\text{L}] + k[\text{N}])$. Therefore $\Lambda = \{k_+(RT/\mathcal{F}v)/(1 + k_-[\text{L-M}_0]/k[\text{N}])b$ which shows that this system depends on two adimensional parameters, $\lambda = k_+(RT/\mathcal{F}v)$ and $\kappa = (k/k_-)([\text{N}]/[\text{L-M}_0])$. For mechanism D_r, $[\text{M}^+]$ is in the steady state as in mechanism D_i and $\S = \{k_+k_+'[\text{L-M}^+][\text{N}] - k_-k_-'[\text{N-M}^+][\text{L}]\}/\{k_-[\text{L}] + k_+'[\text{N}]\}$, i.e.,

$$\Lambda = \{k_+k_+'[\text{N}](RT/\mathcal{F}v)b - k_-k_-'[\text{L-M}_0]cl\}/\{k_-[\text{L-M}_0]l + k_+'[\text{N}]\}$$

or

$$\Lambda = \{k + (RT/\mathcal{F}v)b - k_-'(RT/\mathcal{F}v) \times [k_-/k_+'[\text{L-M0}]/[\text{N}]]cl\}/\{1 + k_-/k_+'[\text{L-M}_0]\}$$

Thus, this system depends on three adimensional parameters, $\lambda = k_+(RT/\mathcal{F}v)$, $\lambda' = k_-'(RT/\mathcal{F}v)$, and $\kappa = (k_+'/k_-)[\text{N}]/[\text{L-M}_0])$. For

(68) Bard, A. J.; Faulkner, L. R. "Electrochemical Methods"; Wiley: New York, 1980.

mechanism I, two different kinetics behaviors are possible according to the magnitudes of k and k_-. When k is not smaller than k_-, $[L-M, N]^+$ will be in the steady state and § is simply expressed as § = $\{kk_+/(k + k_-)\}[L-M^+][N]$ since the steady state condition will apply to $[N-M, L]^+$. This is the same formulation as that for A_i, and the system will depend only on one adimensional parameter, $\lambda = \{kk_+/(k + k_-)\}[N](RT/\mathcal{F}v)$. $+ k_-)\}[N](RT/\mathcal{F}v)$. On the other hand, when k is smaller than k_-, eq 25 will be in fast equilibrium and $[N-M, L]^+$ in the steady state, leading to § = $k[L-M^+]\{k_+/k_-)[N]/[1 + (k_+/k_-)[N]]\}$ which gives $\Lambda = [k-(RT/\mathcal{F}v)]\{(k_+/k_-)[N]/[1 + (k_+/k_-)[N]\}b$. This system thus depends on two adimensional parameters, $\lambda = k(RT/\mathcal{F}v)$ and $\kappa = (k_+/k_-)[N]$, which predict a different effect from variations arising from changes of [N] or v. However, if $(k_+/k_-)[N] \ll 1$, Λ simplifies to $\Lambda = \{k(k_+/k_-)(RT/\mathcal{F}v)[N]\}b$, leading to a dependence of the system on one parameter $\lambda' = k(k_+/k_-)(RT/\mathcal{F}v)[N]$. This last case is indeed included in the above formulation. In other words, the interchange mechanism will appear as two limiting kinetics behaviors—one when $(k_+/k_-)[N]$ is large or ~ 1 and the other when it is less than 1. The former will depend on two parameters, $\lambda = k(RT/\mathcal{F}v)$ and $\kappa = (k_+/k_-)[N]$, and the latter will depend on only one parameter, i.e.,

$$\lambda = k_{ap}(RT/\mathcal{F}v)[N]$$

where $k_{ap} = (k_+k)/(k + k_-)$.

Acknowledgment. We thank Dr. J. W. Hershberger for helpful discussions in the early stages of this research, Professors W. Trogler and F. Basolo for sending us a preprint of their paper[32] prior to publication, the National Science Foundation for financial support, and the United States–France (NSF–CNRS) cooperative program for an award of a fellowship to C.A.

Registry No. η^5-MeCpMn(CO)$_2$(4-MeOpy)$^+$, 89727-37-7; η^5-MeCpMn(CO)$_2$(4-NO$_2$py)$^+$, 89727-38-8; η^5-MeCpMn(CO)$_2$(4-Mepy)$^+$, 89727-44-6; η^5-MeCpMn(CO)$_2$(py)$^+$, 89727-45-7; η^5-MeCpMn(CO)$_2$(4-CH$_3$COpy)$^+$, 89727-46-8; η^5-MeCpMn(CO)$_2$(3-Mepy)$^+$, 89727-47-9; η^5-MeCpMn(CO)$_2$(3-Fpy)$^+$, 89727-48-0; η^5-MeCpMn(CO)$_2$(3-Clpy)$^+$, 89727-49-1; η^5-MeCpMn(CO)$_2$(4-CH$_3$COpy), 60718-84-5; η^5-MeCpMn(CO)$_2$(py), 60718-82-3; η^5-MeCpMn(CO)$_2$(4-MeOpy), 89727-39-9; η^5-MeCpMn(CO)$_2$(4-NO$_2$py), 89727-40-2; η^5-MeCpMn(CO)$_2$(4-Mepy), 60718-81-2; η^5-MeCpMn(CO)$_2$(3-Mepy), 89727-41-3; η^5-MeCpMn(CO)$_2$(3-Fpy), 89727-42-4; η^5-MeCpMn(CO)$_2$(3-Clpy), 89727-43-5; η^5-MeCpMn(CO)$_2$(PEt$_3$), 65152-86-5; η^5-MeCpMn(CO)$_2$(PPh$_2$Me), 37685-57-7; η^5-MeCpMn(CO)$_2$(PPh$_3$), 12100-95-7; η^5-MeCpMn(CO)$_2$(PPh$_2$Et), 89727-50-4; η^5-MeCpMn(CO)$_2$(PPhEt$_2$), 89727-51-5; η^5-MeCpMn(CO)$_2$(P(OMe)Ph$_2$), 83746-92-3; η^5-MeCpMn(CO)$_2$(P(C$_6$H$_4$CH$_3$-p)$_3$), 83746-90-1; η^5-MeCpMn(CO)$_2$(P(C$_6$H$_4$OCH$_3$-p)$_3$), 89727-52-6; η^5-MeCpMn(CO)$_2$(PPh$_2$(n-Bu)), 89727-53-7; η^5-MeCpMn(CO)$_2$(PPh$_2$(i-Pr)), 89727-54-8; η^5-MeCpMn(CO)$_3$, 12108-13-3; P(OMe)Ph$_2$, 4020-99-9; PPhEt$_2$, 1605-53-4; PPh$_2$Et, 607-01-2; PPh$_3$, 603-35-0; PEt$_3$, 554-70-1; P(p-MePh)$_3$, 1038-95-5; P(p-MeOPh)$_3$, 855-38-9; PPh$_2$Me, 1486-28-8; PPh$_2$(n-Bu), 6372-41-4; PPh$_2$(i-Pr), 6372-40-3.

α-Selenocarbenium Ions: Preparation, X-ray Molecular Structure Determination, and ^{1}H and ^{13}C NMR Spectral Characterization†

L. Hevesi,*‡ S. Desauvage,‡ B. Georges,‡ G. Evrard,‡ P. Blanpain,‡ A. Michel,‡ S. Harkema,⊥ and G. J. van Hummel⊥

Contribution from the Department of Chemistry, Facultēs Universitaires Notre-Dame de la Paix, B-5000-Namur, Belgium, and the Chemical Physics Laboratory, Twente University of Technology, 7500 AD Enschede, The Netherlands. *Received January 4, 1984*

Abstract: Bis(methylseleno)carbenium ion salts (I, R = H, Et, PhCH$_2$; Y = BF$_4$, SbCl$_6$) as well as their bis(methylthio) analogues

$$\underset{\text{I}}{RC^+(SeMe)_2\,Y^-} \qquad \underset{\text{II}}{RC^+(SMe)_2\,Y^-}$$

(II, R and Y the same as in I) have been prepared by the reaction of the corresponding orthoseleno- and orthothioesters either with triphenylcarbenium or with appropriate silver salts in dichloromethane. They have been isolated as pure crystalline solids and structurally investigated by NMR and X-ray techniques. Comparison of the results for selenium, sulfur, and oxygen derivatives shows the existence of important mesomeric stabilization of the positive charge in all three types of cations by the unshared electrons of the heteroatomic substituents. The ordering of stabilizing ability of the heteroatoms as obtained from proton chemical shifts (Se > O >S) contrasts with that resulting from ^{13}C and X-ray data (O >S ≃ Se). ^{1}H NMR spectra of bis(methylthio)ethyl-, bis(methylthio)benzyl-, and bis(methylseleno)benzylcarbenium ions were found to be reversibly temperature dependent. This was interpreted as a result of hindered rotation around C$^+$–S and C$^+$–Se bonds having activation energies of 8 ± 2, 14 ± 2, and 13 ± 2 kcal/mol, respectively. The values are comparable to those of the oxocarbenium ions (8–15 kcal/mol), suggesting similar π bonds. X-ray structure determinations carried out on I and II (R = benzyl; Y = SbCl$_6$) reveal substantial shortenings of the C$^+$–Se and C$^+$–S bond distances by 0.15 and 0.14 Å, respectively, as compared to the corresponding single-bond distances in saturated molecules. Estimated π bond orders ($\sim$0.50 for both thio- and selenocarbenium ions and 0.66–0.80 for the oxo derivatives) indicate that delocalization of selenium nonbonded electrons is just as strong as that of sulfur lone pairs in these cationic species.

A large variety of heterosubstituted carbenium ion salts has been described[1] in which the positive charge is stabilized by second-row elements such as nitrogen and oxygen.

The subject of dithiolium ions[2,3] and that of other mono- and dithiocarbenium ions[1,4,5] are now also well documented. However, virtually nothing is known about the possibility and extent of stabilization of carbocations by the fourth-row element selenium.[6] We wish to report here on the easy preparation and some structural

† Presented in part at the International Symposium on "Chemistry of Carbocations", University College of North Wales, Bangor, Sept 7–11, 1981. No reprints of this paper will be available.

‡ Facultēs Universitaires Notre-Dame de la Paix.

⊥ Twente University of Technology.

(1) For a review, see, for example: Pittman, C. U., Jr.; Mac Manus, S. P.; Larsen, J. W. *Chem. Rev.* **1972**, *72*, 357.

(2) Lozach, N.; Stavaux, M. *Adv. Heterocycl. Chem.* **1980**, *27*, 151.

(3) Hirai, K.; Sugimoto, H.; Ishiba, T. *Yuki Gosei Kagaku Kyokaishi* **1981**, 192.

(4) Marino, J. P. In "Topics in Sulfur Chemistry"; Senning, A., Ed.; George Thieme Verlag: Stuttgart, 1976; Vol. 1, p 1, and references cited therein.

(5) Jorritsma, R. Ph.D. Thesis, University of Amsterdam, 1979.

0002-7863/84/1506-3784$01.50/0